An experimental study of a reactive plume in grid turbulence

By R. J. BROWN and R. W. BILGER

Department of Mechanical and Mechatronic Engineering, University of Sydney,
NSW 2006, Australia

Experimental results for a reactive non-buoyant plume of nitric oxide (NO) in a turbulent grid flow doped with ozone (O_3) are presented. The Damköhler number (N_D) for the experiment is of order unity indicating the turbulence and chemistry have similar timescales and both affect the chemical reaction rate. Continuous measurements of two components of velocity using hot-wire anemometry and the two reactants using chemiluminescent analysers have been made. A spatial resolution for the reactants of four Kolmogorov scales has been possible because of the novel design of the experiment. Measurements at this resolution for a reactive plume are not found in the literature. The experiment has been conducted relatively close to the grid in the region where self-similarity of the plume has not yet developed. Statistics of a conserved scalar, deduced from both reactive and non-reactive scalars by conserved scalar theory, are used to establish the mixing field of the plume, which is found to be consistent with theoretical considerations and with those found by other investigators in non-reactive flows. Where appropriate the reactive species means and higher moments, probability density functions, joint statistics and spectra are compared with their respective frozen, equilibrium and reaction-dominated limits deduced from conserved scalar theory. The theoretical limits bracket reactive scalar statistics where this should be so according to conserved scalar theory. Both reactants approach their equilibrium limits with greater distance downstream. In the region of measurement, the plume reactant behaves as the reactant not in excess and the ambient reactant behaves as the reactant in excess. The reactant covariance lies outside its frozen and equilibrium limits for this value of N_D. The reaction rate closure of Toor (1969) is compared with the measured reaction rate. The gradient model is used to obtain turbulent diffusivities from turbulent fluxes. Diffusivity of a non-reactive scalar is found to be close to that measured in non-reactive flows by others.

1. Introduction

Turbulent reacting flows are common in natural and man-made environments. Examples can be found in oceans and lakes, the atmosphere, biological processes, and turbulent combustion. These flows often have complex turbulence and may involve multi-step chemistry. Theoretical or experimental study of this complex process generally requires simplification of the turbulence field, the fluid boundary conditions and the chemistry. The present work applies an accurate, reliable and well-established measuring technique to an experimental configuration that is simplified as follows: simple classical flow which is a point source plume in approximately homogeneous turbulence; a reaction which is passive so that the chemical reaction has insignificant

heat release and does not affect the fluid mechanics; one-step irreversible chemical reaction; and Schmidt numbers (defined later) for the reactants which are very close and near unity. However, the mixing field is not self-preserving because it is relatively close to the turbulence-generating grid.

The aim of the present work is to obtain a well-resolved set of concentration and velocity data that can be used to improve our understanding of turbulent reacting flows and to develop advanced models for computation of these flows.

The important theoretical issues that the present results can throw light on will now be surveyed briefly. Conserved scalar theory (Bilger 1980a, Bilger, Saetran & Krishnamoorthy 1991) leads to considerable simplification of the scalar conservation equations by describing the instantaneous state of mixedness of two fluids in terms of a conserved scalar, to which all other conserved scalars are linearly related. Conserved scalars are quantities such as combinations of temperature and species concentrations that have no chemical source term in their conservation equations. Assumptions involved are low Mach number, adiabatic flow, equal diffusivities of scalars and Lewis number (defined later) (for combusting flows) of unity. These assumptions need to be tested in different flows. For example, the first measurement which showed the effect of Schmidt number (defined later) in shear layer mixing was Breidenthal (1979). Later Koochesfahani & Dimotakis (1986) found that product formation is significantly reduced by Schmidt number effects in reacting-liquid mixing layers. In modelling turbulent transport, simplifications such as the empirical gradient model are known to break down where the scale of the scalar is not sufficiently larger than the scale of the turbulence. While good results have been obtained in grid turbulence this is a special case. Knowledge of the mean reaction rate is essential for models of turbulent reacting flow. In the p.d.f. approach of Pope (1985) this rate is implicit, but there is still the problem that the mixing must be modelled for the correct form of the p.d.f. to be found. Perhaps the simplest approach to find the mean reaction rate is the product of means closure which is known to have large errors because reactant fluctuations are ignored. In the fast chemistry limit of Bilger (1980a), the species are uniquely related to a conserved scalar and the reaction rate is proportional to the mean scalar dissipation conditional on the value of a conserved scalar. This has led to great interest in the joint statistics of a scalar and its dissipation in non-reactive flows (Prasad & Sreenivasan 1990). Other approaches for the mean reaction rate are the reaction-dominated limit (Mell et al. 1994), the Toor (1969) closure, the laminar flamelet model (Peters 1988), the perturbation closure (Bilger 1980b), and the conditional moment closure. The latter was developed independently by Bilger (1993) and Klimenko (1990). They derive scalar conservation equations that are conditioned on the value of a conserved scalar. Fluctuations around the conditional mean reactive scalars are often negligible so that the reaction rate can accurately be found simply from the product of conditional means. The effect of reaction on scalar spectra is also of interest in the study of turbulent reacting flow (Corrsin 1961, 1964). Theory has recently been developed by Kosály (1993) to predict the auto- and cross-spectra of reacting scalar fluctuations.

A significant advance in the experimental study of turbulent reacting flows has been made by Bilger et al. (1991). They developed a technique using a facility known as the Turbulent Smog Chamber to make simultaneous high-resolution measurements of reactant concentrations and turbulent velocities in a turbulent reactive-scalar-mixing layer. Conserved scalar theory was used to characterize the mixing field of the reactants and relate it to experiments by others in non-reactive-scalar-mixing layers. An experiment similar to that of Bilger et al. but using water was con-

ducted by Komori *et al.* (1993). Studies have been conducted in thermal mixing layers in air by LaRue, Libby & Seshadri (1981), Ma & Warhaft (1986), Gibson, Jones & Kanellopoulos (1989) and others. Bilger *et al.* (1991) used their data to test conserved scalar theory, closures for the reaction rate, and the gradient model for the turbulent flux. Their work has provided well-resolved data that have led to the development of the conditional moment closure (Bilger 1993). It has also been used in linear-eddy modelling of turbulent transport with finite rate chemistry by Kerstein (1992), in direct numerical simulations of turbulent reacting flow by Mell *et al.* (1993, 1994) and in theoretical study of reactant spectra by Kosály (1993).

The effects of parameters such as large Schmidt number and large Schmidt number differences are not addressed by the conserved scalar theory. A different approach which addresses this more directly was originally developed by Broadwell & Breidenthal (1982). This was later modified slightly by Broadwell & Mungal (1991) who compiled more recent data to support the model. Comparisons between the two approaches are therefore not made in the present study.

The measurement techniques established by Bilger *et al.* (1991) and Li, Brown & Bilger (1992, 1995) in the reactive-scalar mixing layer and Li & Bilger (1996) in the reactive line source are used in the present work to study the reactive point source of NO in a grid flow of O_3.

A review of reactive and non-reactive plume studies will now be given. In turbulent reactive flow studies NO and O_3 have often been used as reactants because they are readily available and have a simple, well-understood reaction. Experiments using these reactants have been reported by Komori & Ueda (1984) using a jet and a plume of NO in a grid flow of O_3, by Builtjes (1983) in a wind tunnel boundary layer, by Vila-Guerau de Arellano *et al.* (1993), Cheng *et al.* (1986) and Bange (1993) using an aeroplane in the Earth's atmosphere and by Delany *et al.* (1986) using ground-mounted instruments in the Earth's atmosphere. Cheng *et al.* (1986) find that NO_2 production is limited by the rate of mixing at the centre of the plume. Bange (1993) investigates the effects of instrument smoothing and shows that its effect is to apparently increase the timescale of the chemical reaction. Related studies are those done by Shea (1977) of a chemical reaction in a turbulent jet of O_3 released into an atmosphere of NO and by Ibrahim (1987) of a point source of NO released into the wake of two opposed flows of O_3. In general the data from these studies are limited in their temporal and spatial resolution.

Experimental studies of non-reactive plumes are more common than those of reactive plumes and the first seems to have been conducted by Kamp de Feriet (1938) in grid turbulence by releasing small soap bubbles from a point source. Mickelsen (1960) also used a point source in grid turbulence to study the relative importance of molecular diffusion by comparing results for helium and carbon dioxide. Gad-el-Hak & Morton (1979) used a point source of smoke in grid turbulence to measure turbulent fluxes by scattering light from smoke particles to measure relative concentrations and laser-Doppler techniques to measure velocities. More recently Nakamura, Sakai & Miyata (1987) and Tsunoda *et al.* (1993) have made measurements with a spatial resolution close to the Kolmogorov scale using dye solution in grid-generated water turbulence. Britter *et al.* (1983) have studied the effect of stable stratification on turbulent diffusion from a point source in grid turbulence. Gehrke & Bremhorst (1993) and Bremhorst *et al.* (1989) studied the temperature field downstream of a multi-bore jet block in which one jet is heated. The multi-bore jet block is analogous to a grid flow. Turbulent pipe flow provides a region of turbulence at its core that has

been used to study turbulent diffusion from a point source by Nye & Brodkey (1967) and others. Fackrell & Robins (1982) used a neutrally buoyant mixture of propane and helium in a laboratory boundary layer. Sawford, Frost & Allan (1985) and Mylne & Mason (1991) measured concentration statistics from ground-level point sources in atmospheric turbulence.

The plan of the paper is as follows. The experimental equipment is described and its resolution is discussed and shown to be adequate. Results are then presented for the flow field to show that it is independent of the cross-stream coordinate. The mixing field is analysed and compared to mixing fields in non-reactive flows measured by others, by the use of statistics of a conserved scalar, F (defined below), which can be derived from normalized non-reactive scalars or from reactive scalars. Statistics of reactive scalars are compared with their equilibrium and frozen limits derived by conserved scalar theory (Bilger *et al.* 1991). Probability density functions (p.d.f.s) of conserved and reactive scalars are presented followed by species covariance and reaction rate closures. Spectra are calculated for conserved and reactive scalars. Turbulent fluxes are used to check the reliability of the measurements by ensuring they are consistent with conservation considerations. They are then used to calculate the turbulent diffusivities and to estimate the dissipation of the conserved scalar variance.

2. Experimental method

The experimental facility for this study has been specially developed to allow simultaneous measurement of reactive scalars and velocities with good spatial and temporal resolution. Measurements at the current resolution for a reactive plume are not found in the literature.

The present experimental method is similar to that used by Bilger *et al.* (1991), Li *et al.* (1992, 1995) and Li & Bilger (1996) in the Turbulent Smog Chamber. Measurements are made in a wind tunnel using laboratory air as shown schematically in figure 1. The walls are constructed from polyethylene and an overpressure of about 100 Pa maintains a constant circular cross-section. The polyethylene walls have been shown to be essentially non-reactive to O_3 (Mudford & Bilger 1983). A square grid made from square bars 65 mm × 65 mm and of pitch $M = 320$ mm generates the turbulence at the entry of the working section which is 2.8 m in diameter and 8 m long. The solidity of the grid is 35%. Details of the initial conditions of each experiment can be found in table 1. The nominal mean axial velocity of the flow ($\overline{U}$) is 0.5 m s^{-1}, giving a Reynolds number $Re = \overline{U}M/v = 10700$, where v is the kinematic viscosity. The turbulence Reynolds number at $x/M = 7$ is $Re_t = u'L_\epsilon/v = 420$, where L_ϵ is the integral lengthscale of the turbulence (an estimate for L_ϵ is made in §3.1). The point source has a diameter $d_{ps} = 31.5$ mm and is located at the centre of the working section at a distance $x_0 = 3M$ from the grid. The main flow (stream 2) is doped with O_3 at the fan intake and is well mixed by the time it reaches the grid, having passed through three right-angle bends, and $\Gamma_{O_3,2} \approx 1$ p.p.m., where Γ_i is the mole fraction of species i. The velocity of the point source, U_{ps}, (stream 1) is matched to $\overline{U}$ and consists of N_2 doped with NO, $\Gamma_{NO,1} = 515$ p.p.m. The reactants undergo the reaction NO+O_3 →NO$_2$+O_2+200 kJ(mol)$^{-1}$ with reaction rate constant, $k = 0.37$ p.p.m.$^{-1}$s^{-1} at 25 °C and 1 atm. In the absence of ultraviolet light the reaction is irreversible. The heat release at the concentrations used causes negligible rise in temperature. The diffusion coefficients at these conditions are $\mathscr{D}_{NO} = 0.18, \mathscr{D}_{O_3} = 0.22$ and $\mathscr{D}_{conserved\,scalar} = 0.20$ cm^2 s^{-1}.

Turbulence grid

$M = 320$ mm

65 mm

$d = 31.5$ mm

$3M$

Instantaneous plume

r

x

Point source $\Gamma_{NO,1}$

$\Gamma_{O_3,2}$

$\bar{\Gamma}_{NO_2}$

$\bar{\Gamma}_{NO}$

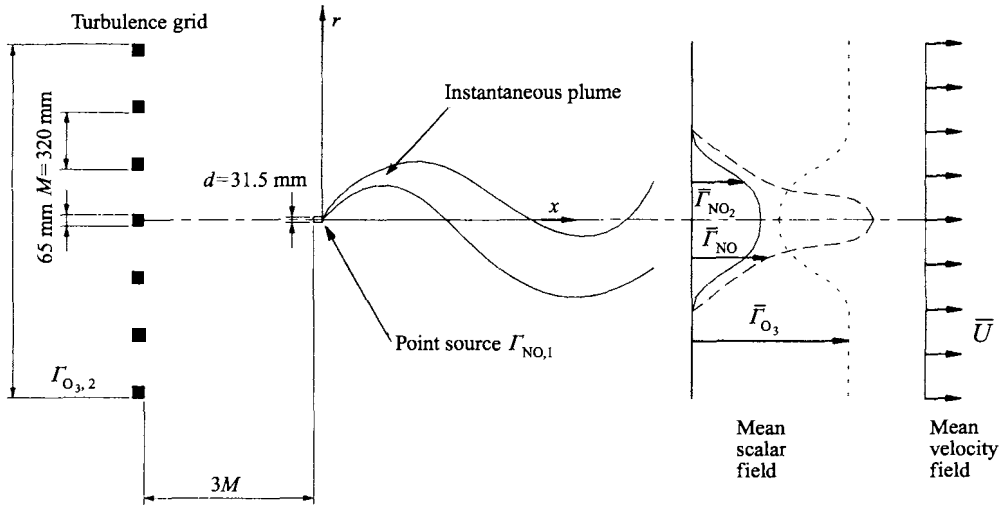$\bar{\Gamma}_{O_3}$

Mean scalar field

$\bar{U}$

Mean velocity field

FIGURE 1. Schematic diagram of experimental facility.

Symbol	Samples per channel	$\Gamma_{NO,1}$ (p.p.m.)	$\Gamma_{O_3,2}$ (p.p.m.)	$\bar{U}$ (m s^{-1})	x/M	σ_m (mm)	Profile orientation	Date (all 1993)
A	2^{13}	515.0	-	0.479	9	167	Horizontal	March 23
B	2^{13}	515.0	-	0.485	9	151	Horizontal	March 8
C	2^{14}	515.0	-	0.471	12	162	Horizontal	February 9
D	2^{13}	515.0	-	0.518	15	189	Horizontal	April 3
E	2^{13}	515.0	-	0.496	17	214	Horizontal	March 10
F	2^{13}	515.0	-	0.574	7	137	Vertical	March 9
G	2^{15}	515.0	-	0.516	9	141	Vertical	January 27
H	2^{13}	515.0	-	0.525	9	160	Vertical	March 23
I	2^{13}	515.0	-	0.529	15	208	Vertical	April 3
J	2^{15}	515.0	1.074	0.506	7	127	Horizontal	April 10
K	2^{15}	515.0	0.988	0.495	9	158	Horizontal	April 7
L	2^{15}	515.0	0.947	0.498	17	206	Horizontal	April 6
M	2^{15}	515.0	1.016	0.543	7	131	Vertical	April 10
N	2^{15}	515.0	1.005	0.534	9	157	Vertical	April 7
O	2^{15}	515.0	1.050	0.529	12	181	Vertical	April 3
P	2^{15}	515.0	1.024	0.531	15	207	Vertical	April 3

TABLE 1. Experimental conditions.

Good spatial and temporal resolution is possible because of the careful selection of the flow parameters for the experiment. The mean velocity is kept low so the Kolmogorov scale will be relatively large. The pitch of the grid is large enough to bring the Reynolds number up to an adequate level. The present experimental set-up is a compromise between the need for having a known turbulence field at a reasonably high Re, measurement stations as far downstream as possible, Damköhler numbers (defined later) of order unity, achieving enough spatial and temporal resolution for the analysers and a limited budget.

Velocity components in the axial and radial directions were measured by a constant-temperature hot-wire anemometer. Simultaneous 4-channel point measurements (two components of velocity and two reactants) were taken across the flow at different

stations downstream of the point source. The hot-wire and gas sampling probes were placed at the same axial location 18 mm apart in the radial direction which caused no interference in the measured flow field. Data are passed through a 50 Hz low-pass filter and sampled at 128 Hz using a 12 bit A/D converter. The number of samples for each point measurement was between 2^{13} and 2^{15} per channel, which corresponds to sampling times of 1 and 4 minutes, respectively (full details in table 1). All data processing is performed on 486 PCs.

The two velocity components were measured by a constant-temperature hot-wire anemometer using an X-wire probe. Calibration was done statically using a TSI 1125 calibrator and a third-order polynomial was fitted to the calibration data. The hot wires were recalibrated after each experiment and drift was found to be negligible.

The dual chemiluminescent analysers used to measure the high-frequency fluctuations of NO and O_3 were originally developed by Mudford & Bilger (1983) and later modified by Bilger *et al.* (1991). Those presently in use are essentially the same as that used by Li *et al.* (1992, 1995). The r.m.s. fluctuation of each analyser due to instrument noise is approximately 0.03 p.p.m. This noise is not a function of the measured concentration. The gas sample flow through each reaction chamber, Q_{sample}, is 70 std cm^3 s^{-1}. Sampling is through a Teflon tube 2.8 mm in diameter and 3.1 m long with a sonic nozzle at the inlet. The delay time and reaction in the tube are compensated for in data processing (Bilger *et al.*, 1991). The flow rate for each reactant in excess for the chemiluminescent analysers, Q_{excess}, is 87 std cm^{3}s^{-1} and each reaction chamber has a volume, $V_{chamber}$, of 32 cm^3 and operates at a pressure of 3.5 kPa(absolute). Using the volume and pressure in front of the photomultiplier tube and the flow rates of the sample and reactants in excess, the spatial resolution of the present system is estimated as $l = 9.8$ mm assuming a spherical form for the flow around the sonic nozzle according to the equation:

$$\frac{4}{3}\pi \left(\frac{l}{2}\right)^3 = V_{chamber}\frac{Q_{sample}}{(Q_{sample} + Q_{excess})}\frac{P_{cell}}{P_{atm}}. \tag{1}$$

The estimated spatial resolution is approximately four times the Kolmogorov scale for this flow (§3.1). The NO calibration was done using a gas cylinder of known concentration and diluted with precision flow meters. The O_3 calibration was done by titration with NO according to the method of Post & Kewley (1978). Straight lines were fitted to the NO and O_3 calibration data by the method of least squares.

The frequency response of the chemiluminescent analysers was measured to be approximately 20 Hz by the method initially described by Mudford & Bilger (1983) and later used by Bilger *et al.* (1991), which uses signal processing theory from Bendat & Piersol (1971).

In order to confirm that a 20 Hz frequency response was adequate to measure the quantities of interest, the data were passed through a 10 Hz third-order low-pass digital filter and reprocessed. Variance, skewness (S) and kurtosis (K) of both reactants were found to drop by no more than 3% on the centreline. The loss in the reactant variances is as expected from the reactant spectra (presented later), where 10 Hz is seen to be nearly two decades down the reactant spectrum. At two decades down the spectrum a loss of variance of the order of 1% would be expected. The probability density functions of the reactants and the conserved scalar were also recalculated using the low-pass filtered data and no observable differences were found. In addition to checking that the frequency response of the chemiluminescent analysers is adequate, it is also necessary to quantify the effects

of spatial averaging. The effect of such resolution on scalar measurements has been quantitatively investigated by Mansour, Bilger & Dibble (1990). Their investigation concerned Raman/Rayleigh laser measurements in turbulent flames but has general application to other physical measuring systems. They assume the Pao–Corrsin scalar spectrum and isotropic flow which is approximated by the present experiment. They find that the error in the scalar variance depends on the probe length relative to both the integral lengthscale and the scalar microscale. For the conditions of this experiment their analysis shows that the loss of scalar variance with a spatial resolution of $l = 10$ mm, found from (1), should be less than 2%. If l is increased to 20 mm the loss of scalar variance does not exceed 5%. Mansour *et al.* also investigate the effect of varying the spatial resolution on the shapes of the scalar probability density functions. Their results show that for spatial resolutions close to that of the present experiment little change in the shape of the p.d.f. would be expected, other than to reduce any sharp peak. In summary, it is concluded that the frequency response and spatial resolution of the chemiluminescent analysers is adequate to measure the quantities of interest in this investigation including higher moments of the reactants.

3. Results

A cylindrical coordinate system is used to present the data with the point source as the origin. The axial and corrected radial coordinates are denoted by x and r, and their instantaneous velocities by U and V, respectively. Unprocessed experimental data were collected using the radial coordinate r'' which was corrected by δ, the shift in the mean plume centreline as explained in §3.2. All experimental profiles traverse the full width of the plume and are shown on the figures to emphasize symmetry. Consequently an apparently negative radius appears on the figures. Instantaneous values are denoted by upper case, e.g. $\Gamma(x,r,t)$ with means denoted by overbars and fluctuating components by lower case, e.g. $\gamma(x,r,t) = \Gamma(x,r,t) - \overline{\Gamma}(x,r)$. Root mean square values are indicated by primes, e.g. $\gamma' = (\overline{\gamma^2})^{1/2}$.

3.1. *Flow field*

The flow field in the test section is that of normal grid flow, i.e. the statistics of the velocity do not vary significantly in the radial direction. The measured mean velocity ($\overline{U} \approx 0.5$ m s^{-1}) is approximately constant for each experimental profile and is shown in table 1. The typical standard deviation of $\overline{U}$ across the flow is 3% of the mean. An example of a mean velocity profile at $x/M = 7$ ($10M$ from the turbulence-generating grid) is shown in figure 2(a). Figure 2(b) shows a profile of the Reynolds stress, $\overline{uv}/(u'v')$, at $x/M = 7$. Radial coordinates in figure 2 are normalized by M to show their position in relation to the grid bars (later radial profiles are normalized by σ_m, defined below). The figure shows a $4M$ wide transverse profile through the wind tunnel centred on its centreline. This width corresponds to approximately half the width of the wind tunnel. While some scatter is seen in $\overline{uv}/(u'v')$ and $\overline{U}$ it does not correspond to the grid bars (located at $r/M = -2, -1, 0, 1, 2$) indicating that there is no effect from irrotational wakes behind the grid bars at this location. The measured turbulence intensity profiles for $u'/\overline{U}$, $v'/\overline{U}$ and $v_2'/\overline{U}$ are approximately constant with typical standard deviations across the flow at $x/M = 7$ of 5% of the average intensities. Here v_2 denotes a radial velocity fluctuation orthogonal to the direction of u and v. The decay of the axial and radial mean-square velocity fluctuations, $\overline{u^2}$
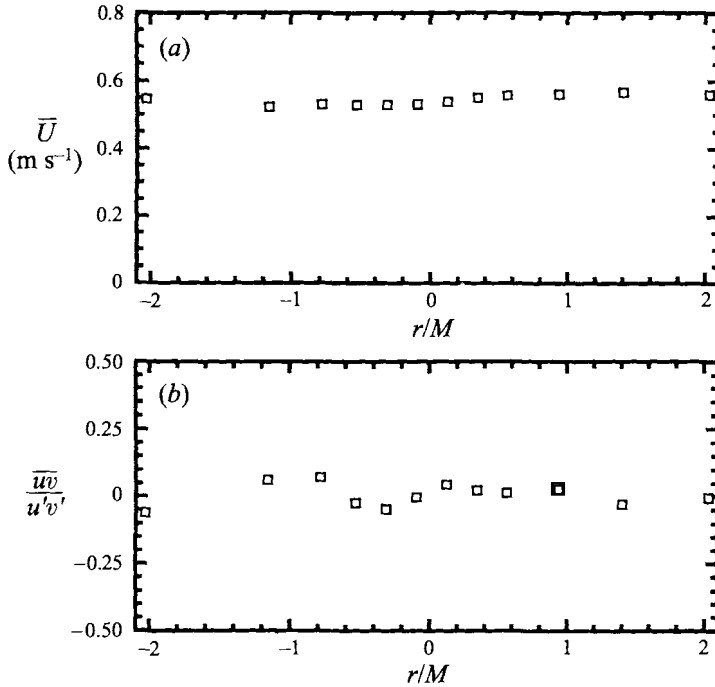
FIGURE 2. Profiles of velocity statistics at $x/M=7$: (a) mean velocity, $\overline{U}$; (b) Reynolds stress, $\overline{uv}/(u'v')$.

and $\overline{v^2}$, respectively, are shown in figure 3. Decay laws fitted to the data are

$$\frac{\overline{u^2}}{\overline{U^2}} = 0.173 \left(\frac{x}{M}\right)^{-1.37}, \qquad \frac{\overline{v^2}}{\overline{U^2}} = 0.041 \left(\frac{x}{M}\right)^{-1.27}.$$

The measured decay is similar to that of Warhaft (1984). The flow is anisotropic with $u'/v' \approx u'/v_2' \approx 1.8$ as shown in figure 3. The flow shows no trend towards an isotropic condition because the region of measurement is relatively close to the grid. At all measurement locations $v'/v_2' \approx 1$ which is necessary for the plume to spread uniformly in all radial directions and to ensure an axisymetric diffusion condition. The boundary layer which develops along the wind tunnel walls does not reach the plume in the length of the working section.

In the range of axial measurements ($x/M = 7$ to 17) the turbulent kinetic energy, defined as $k_t = \frac{1}{2}(u'^2 + v'^2 + v_2'^2)$, varies from 1.45×10^{-3} to 5.74×10^{-4} m^{2}s^{-2}. Its dissipation obtained from $\epsilon = -\overline{U}\mathrm{d}k_t/\mathrm{d}x$, varies from 3.19×10^{-4} to 6.16×10^{-5} m^{2}s^{-3} over the range of measurements. These values give estimates for the integral scale, $L_\epsilon = k_t^{3/2}/\epsilon$, of 170 and 220 mm and the Kolmogorov scale, $\eta = (v^3/\epsilon)^{1/4}$, of 1.8 and 2.7 mm, at $x/M = 7$ and 17, respectively.

The injection velocity of the point source is adjusted to match that of the mean flow and no velocity deficit is observed in the velocity profiles at the axial measurement stations. The spectra of the velocity at $x/M = 7$ show no observable differences at various radial locations which indicates that the point source has caused minimal disturbance to the flow. Typical spectra for u and v are shown in figure 4. The point source measurements of Nakamura *et al.* (1987) have a point source velocity 1 to 1.5 times that of the mean velocity, while Komori & Ueda (1984) used a ratio of 1 and
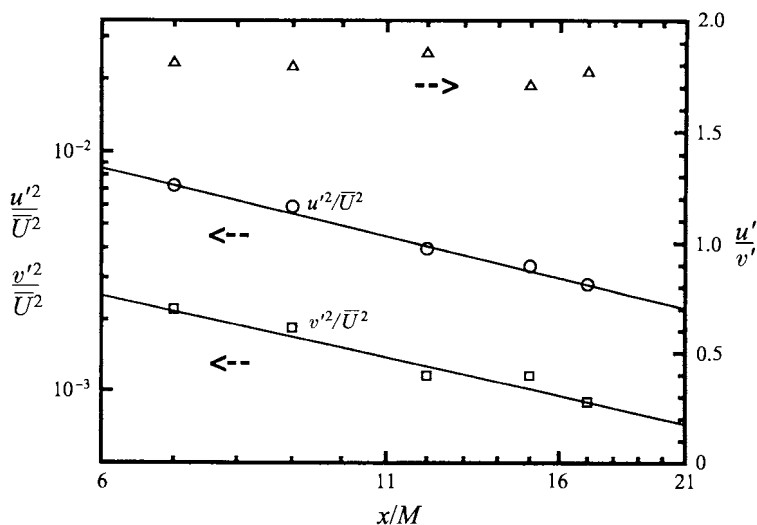
FIGURE 3. The decay of the longitudinal velocity variance, $\overline{u^2}$, the cross-stream variance, $\overline{v^2}$, and the anisotropy, u'/v': $\circ$, $\overline{u^2}/\overline{U}^2$; $\square$, $\overline{v^2}/\overline{U}^2$; $\triangle$, u'/v'.
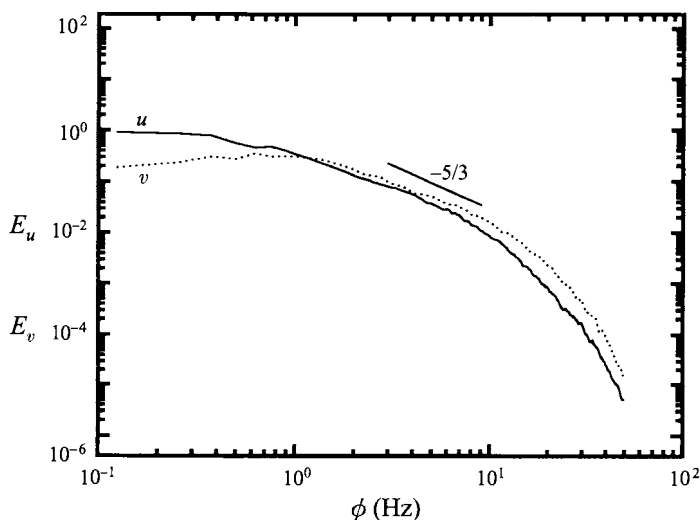

FIGURE 4. Spectra of u and v at $x/M = 7$. A line of slope $-\frac{5}{3}$ is also shown.

Gad-el-Hak & Morton (1979) used a ratio of 2.5. The latter high value may explain some differences between their results and those obtained in the present experiment, as discussed later.

3.2. Mixing field

The mixing of the plume with the surrounding fluid can be described in terms of a suitably defined conserved scalar. Since the system is passive the mixing found here should show agreement with measurements and theory for non-reacting scalar mixing. Such comparisons make it possible to validate the experimental procedures used here. Conserved scalars obtained in this way are linearly related to all other conserved scalars in the flow provided the Lewis number $(= \alpha/\mathscr{D})$ is unity, where α is
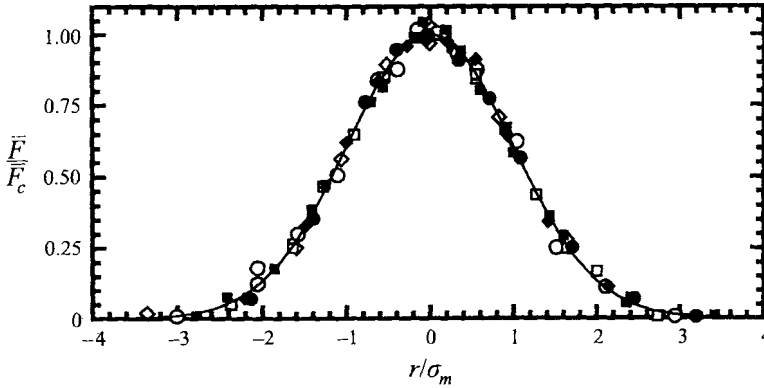
FIGURE 5. Profiles of mean mixture fraction at $x/M = 7$, 15 and 17. The full curve is the Gaussian function. Symbols for all subsequent figures are, unless otherwise stated: open symbols, reactive experiments; full symbols, non-reactive experiments: □, $x/M = 7$; △, $x/M = 9$; ▽, $x/M = 12$; ◇, $x/M = 15$; ○, $x/M = 17$.

the thermal diffusivity for all species i. The statistics of the mixing field are important in generating the limits to reactant scalar statistics given by conserved scalar theory.

The quantity $\Gamma_{NO} - \Gamma_{O_3}$ is a conserved scalar with no chemical source term. Such variables are sometimes known as Shvab–Zel'dovich functions. They can be used to define a conserved scalar referred to hereinafter as the mixture fraction,

$$F = \frac{\Gamma_{NO} - \Gamma_{O_3} + \Gamma_{O_3,2}}{\Gamma_{NO,1} + \Gamma_{O_3,2}}, \tag{2}$$

where subscripts 1 and 2 denote unmixed conditions in the plume and the grid flow, respectively. The mixture fraction has a value of zero in the unmixed O_3 stream and a value of unity in the unmixed NO stream.

Figure 5 shows cross-stream profiles of mean mixture fraction, $\overline{F}$, from reactive and non-reactive experiments at various stations in the flow. The centreline mean mixture fraction $\overline{F}_c$ has been used as the normalizing variable. The Gaussian function

$$\overline{F} = \overline{F}_c \exp\left\{ -\frac{1}{2} \left(\frac{r'' - \delta}{\sigma_m} \right)^2 \right\} \tag{3}$$

was assumed for each profile. The values of $\overline{F}_c$, σ_m, the standard deviation of the mean plume $\overline{F}$ profile and δ, the shift in the mean plume centreline, were obtained by least-squares fitting to each profile. A correction $r = r'' - \delta$ was made to all profiles presented in the figures so that $r = 0$ at the radial location of $\overline{F}_c$. The range of δ was less than 30 mm over all the profiles presented in the figures. This is considered quite acceptable in view of the much larger dimension of the plume. The normalized $\overline{F}$ data in figure 5 collapse well onto the plotted Gaussian curve $\overline{F}/\overline{F}_c = \exp\{-\frac{1}{2}(r/\sigma_m)^2\}$. The grid-turbulence experimental results of Nakamura *et al.* (1987) in water and Komori & Ueda (1984) in air also collapse onto Gaussian curves.

Figure 6 shows the axial decay of the centreline mean mixture fraction, $\overline{F}_c$ and the centreline r.m.s. mixture fraction, $f'_c = \overline{f_c^2}^{1/2}$. Empirical decay laws

$$\overline{F}_c = K_F \left(\frac{x}{M} \right)^{-1}, \qquad f'_c = K_f \left(\frac{x}{M} \right)^{-1.32} \tag{4}$$
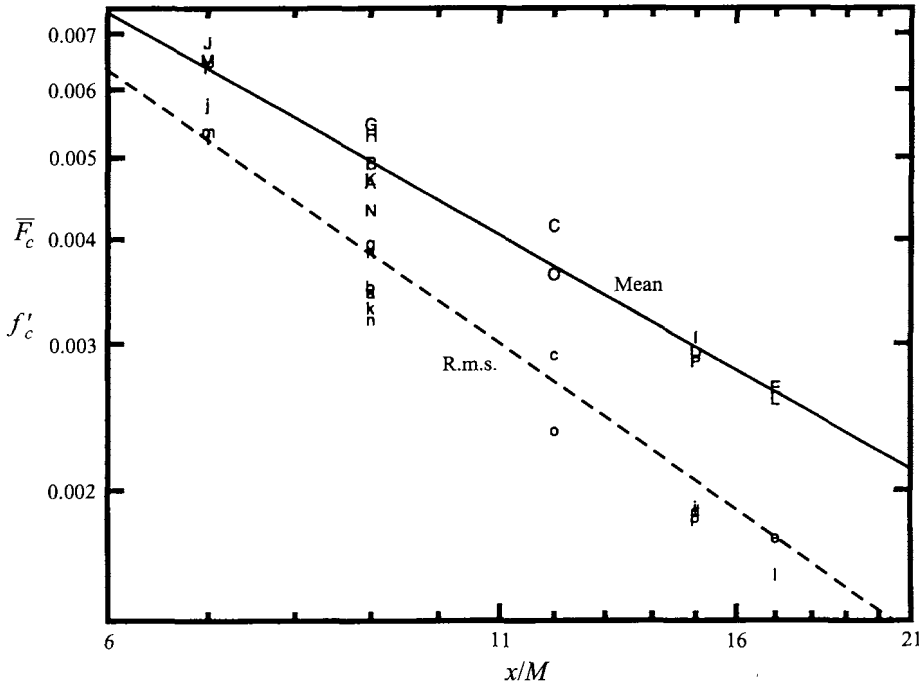
FIGURE 6. Axial decay of the centreline mean and r.m.s. mixture fraction. Symbols as in table 1: upper case, mean; lower case, r.m.s. The decay laws (4) are also shown.

are fitted to the data without the use of a virtual origin. Constants $K_F = 0.0445$ and $K_f = 0.0674$ give the best fit for these data.

The exponent in (4) for the decay of the mean centreline mixture fraction was also found to be -1 by both Komori & Ueda (1984) and Nakamura *et al.* (1987). The lack of need for a virtual origin may be due to the placement of the point source downstream of the grid at $x_0 = 3M$ rather than at $x_0 = 2M$ or $1.5M$ as Nakamura *et al.* (1987) did in a dye plume in water, or at $x/M = 0$ as Komori & Ueda (1984) did in thermal and concentration plumes in air. They found virtual origins of $3M$ and $2M$, respectively. Placement of the point source at $x_0 = 0$ causes the plume to commence its development in a region of complex developing turbulence. Grid turbulence develops relatively quickly downstream of the grid. Jayesh & Warhaft (1992) have found that by $x/M = 4$ the axial velocity intensity behind the grid bar and at the centre of the mesh, between the bars, become equal. The location of the point source in the present experiment is close to this distance at $x/M = 3$. The results of this experiment support the view that placement of the point source at such a location may reduce the need of a virtual origin.

The standard deviation of the $\overline{F}$ profile, σ_m, which is a measure of the growth of the mean plume, is shown in figure 7 and was found to follow the power law

$$\sigma_m/M = K_{\sigma_m} \left(\frac{x}{M}\right)^{1/2} \tag{5}$$

with $K_{\sigma_m} = 0.160$ giving the best fit for these data. The data show some scatter and it appears that at the lower values of x/M the remnants of the turbulent convective stage of the plume (defined below), where σ_m develops as (x/M), are still present. The exponent of $\frac{1}{2}$ is as expected from an assumption of conservation of mixture fraction
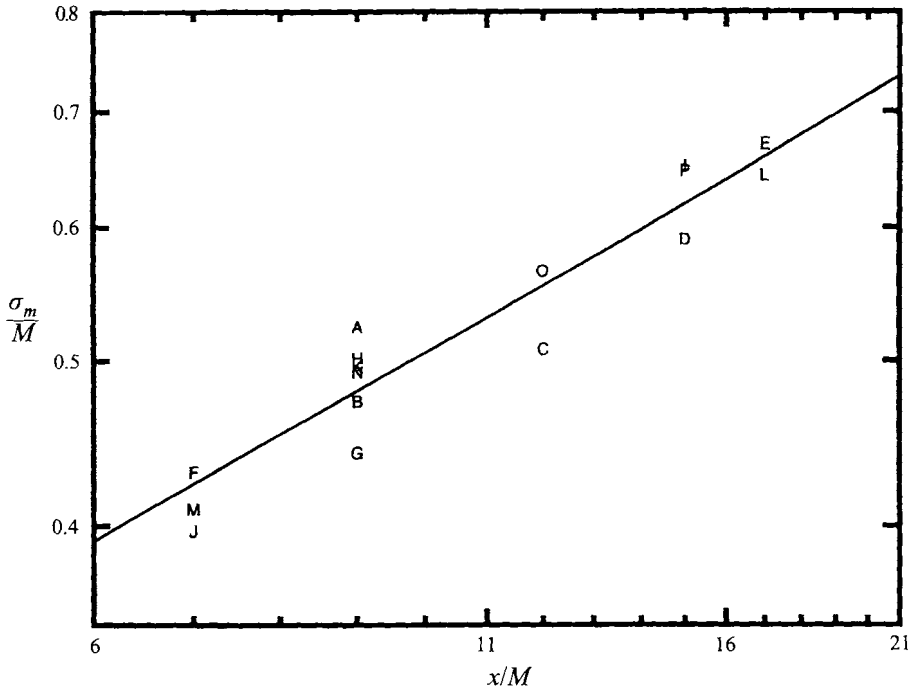
FIGURE 7. Axial growth of the standard deviation of the mean plume. Symbols as in table 1. The power law (5) is also shown.

for $\bar{F}_c$ having a decay exponent of -1. Nakamura *et al.* and Komori & Ueda both find growth exponents of $\frac{1}{2}$.

It was originally recognized by Taylor (1921) that there are three stages in the evolution of a plume. In high Reynolds number, non-decaying, homogeneous turbulence the stages are:

Molecular diffusion,	$t \ll D/\overline{v^2}$,	$\sigma_m \propto t^{1/2}$;
Turbulent convection,	$D/\overline{v^2} \ll t \ll t_L$,	$\sigma_m \propto t$;
Turbulent diffusion,	$t \gg t_L$,	$\sigma_m \propto t^{1/2}$;

where t_L is the Lagrangian timescale. The present flow is decaying grid turbulence but Taylor's theoretical basis for understanding the development of the plume has been applied to this type of flow by Anand & Pope (1985), Warhaft (1984) and Stapountzis *et al.* (1986) who studied thermal line sources in grid turbulence. The physical dimensions of the point source exceed that of the Kolmogorov scale so that the present plume does not have a molecular diffusion stage. In the region of measurement, $x/M = 7$ to 17, $t > t_L$ indicating that the plume is in the turbulent diffusive stage.

By the use of either Prandtl's mixing-length theory or the assumption of self-preservation of the scalar field, turbulent diffusivity can be expressed as $D_{t,f} = \text{const} \times v'L_\epsilon$. In grid-generated flow, turbulence decays downstream and so turbulent diffusivity will also change. However, from §3.1, $v'L_\epsilon$ is found to be a weak function of axial distance which goes as $(x/M)^{0.3}$. This represents a change in turbulent diffusivity of less than 30% in the range $x/M = 7$ to 17. Normalization of turbulent diffusivity will not be by $v'L_\epsilon$ because of its small change with axial distance. In keeping with

most other descriptions of scalar transport in grid turbulence and to make direct comparisons with other experimental results, normalization will be by $\overline{U}M$, denoted as $\hat{D}_{t,f} = D_{t,f}/(\overline{U}M)$.

Taylor's diffusion theory may be used to estimate $\hat{D}_{t,f}$. By assuming long diffusion times the relation (Hinze 1975)

$$\sigma_m^2 = \frac{2D_{t,f}}{\overline{U}}(x - x^*) \tag{6}$$

is obtained, where x^* is the x-coordinate of a virtual origin for the spread of σ_m^2, which in this case was found to be negligible. Using (5) and (6) and normalizing by $\overline{U}$ and M a value of $\hat{D}_{t,f} = 0.0128$ was obtained. Komori & Ueda (1984) using a thermal air plume in grid turbulence ($x/M = 18$ for $M = 30$ mm; present experiment $M = 320$ mm) and the gradient model obtain values of $\hat{D}_{t,f}$ in the range 0.012 to 0.017. Their results are somewhat higher than the present results. Nakamura *et al.* (1987) in a water plume ($26.5 \leqslant x/M \leqslant 80$ for $M = 10$ mm and $13.5 \leqslant x/M \leqslant 40$ for 20 mm) use Taylor's diffusion theory from which $\hat{D}_{t,f}$ can be found to be 0.00442 and 0.00531, respectively. The intensity of their velocity, $u'/\overline{U}$, was within 20% of that found in the present experiment. Although the values are lower by a factor of about 2 than those obtained in the present experiment, they are quite close considering the differences in the fluid properties and the measurement techniques used in each experiment. In the scalar mixing layer of Bilger *et al.* (1991) maximum values of $\hat{D}_{t,f}$ occur on the centreline and are found to be about 0.017, which is slightly higher than that found in the present study.

The constant, K_F, in (4) for the decay of the mean centreline mixture fraction can be related to the turbulent diffusivity, $D_{t,f}$. Nakamura *et al.* (1987) have shown that

$$K_F = \frac{d_{ps}^2 U_{ps}}{16 D_{t,f} M} \tag{7}$$

assuming similarity of the mixture fraction mean and flux fields and the gradient-type model of diffusion (the form of (7) in Nakamura *et al.* contains a typographical error which has been corrected here). Equation (7) assumes a constant value of turbulent diffusivity, which, as explained above, is approximated in the present flow. The value of K_F from (7), using the $\hat{D}_{t,f} = 0.128$ obtained from (6), is 0.047 which is quite close to the experimentally determined value of 0.0445 from (4).

The equivalent source strength, Q, was calculated for each profile as a check on the measurements. Noting that the mean velocity, $\overline{U}$, is constant and that $\overline{uf}$ makes no significant contribution to Q, we have,

$$Q = 2\pi\overline{U} \int_0^\infty r\overline{F}dr. \tag{8}$$

$\hat{Q}$ is obtained by normalizing by the source strength, Q_0, that is the value of Q at $x = 0$. The point source has a top-hat distribution and so $Q_0 = \frac{1}{4}\pi d_{ps}^2 U_{ps}$, noting that at $x = 0$, $\overline{F} = 1$ by definition. Mixture fraction is a conserved quantity and so $\hat{Q}$ should have the constant value of unity at any axial location. Values of $\hat{Q}$ were found to vary from 1.08 to 0.82 with a mean of 0.95. Two factors contribute to this scatter in $\hat{Q}$ because they affect the calculation of $\overline{F}$. First, the low and less accurate Γ_{NO} values that occur at large radii contribute significantly to the error in $\hat{Q}$ because it is weighted in the integrand of (8) by r. Secondly, drift in the chemiluminescent analysers, though small relative to $\Gamma_{O_{3,2}}$, will shift the calculation of mixture fraction
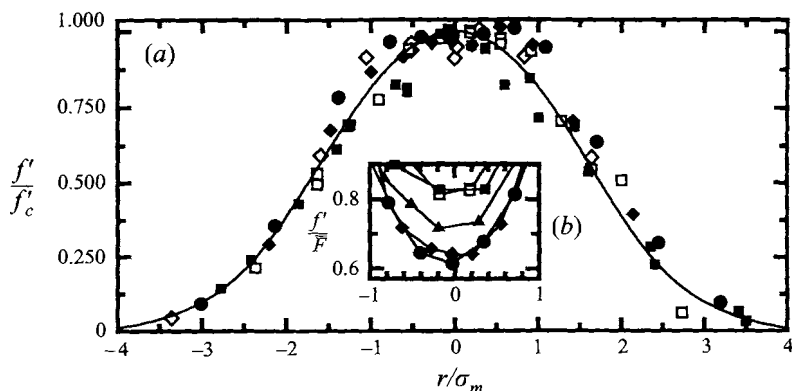
FIGURE 8. (a) Profiles of r.m.s. value of mixture fraction at $x/M = 7$, 15 and 17. The full curve shows data of Nakamura et al. (1987). Symbols as in figure 5. (b) Profiles of the r.m.s. of the mixture fraction in the centreline region normalized by local mean mixture fraction, $f'/\overline{F}$, at $x/M = 7$, 9, 15 and 17.

from (2) because the numerator contains the term $(-\Gamma_{O_3} + \Gamma_{O_3,2})$. For example, where Γ_{O_3} is, say, 90% of $\Gamma_{O_3,2}$, a 1% drift in the chemiluminescent analyser will cause a 10% error in $(-\Gamma_{O_3} + \Gamma_{O_3,2})$. Both analysers were calibrated before and after experiments. Drift from the calibration used for either analyser during experiments was less than 2% of $\Gamma_{O_3,2}$. The scatter in $\hat{Q}$ from non-reactive and reactive experiments shows no observable differences.

Figure 8(a) shows profiles of the r.m.s. of the mixture fraction, f' normalized by f'_c. Data of Nakamura et al. (1987) from a plume of dye solution in grid-generated water turbulence in the region $13.25 \leqslant x/M \leqslant 40$ are also plotted. The point source in their experiments was located at $x_0 = 0$ and a virtual origin of $3M$ downstream of the grid was used. The two sets of data generally show the same features, although those of Nakamura et al. have greater self-similarity, and this is attributable to them being at a location further downstream.

Figure 8(b) shows profiles of the intensity of fluctuation in the centreline region at all axial locations except $x/M = 12$, which is omitted for clarity. The intensity is the r.m.s. of the mixture fraction normalized by local mean mixture fraction, $f'/\overline{F}$. The variation on the centreline from 0.8 at $x/M = 7$ to 0.6 at $x/M = 17$ shows that self-similarity has not been reached. There are limited data available on the moments of a scalar dispersing from a point source. For this reason data in figures 8(b) and 9 (described below) will be compared to point sources released in boundary layers. Fackrell & Robins (1982) made wind tunnel measurements of intensity and found a centreline value of 0.6 using a ground-level neutrally buoyant plume of propane and helium in a boundary layer. Sawford (1987) made ground-level measurements of a plume in the atmospheric boundary layer and found the intensity on the centreline to be approximately 1.0. Values of intensity in the present experiment are consistent with those obtained by the other investigators considering the differences in the types of flow.

Figure 9 shows profiles of skewness, $S = \overline{f^3}/f'^3$ and kurtosis, $K = \overline{f^4}/f'^4$ at $x/M = 7$ and 17. Profiles at other locations ($x/M = 9$, 12 and 15) show a similar trend. There is no observable difference for f', S and K derived from reactive and non-reactive experiments. S and K both show significant departures from the Gaussian values of $S = 0$ and $K = 3$, particularly away from the centreline. Sawford (1987) has measured S and K for a plume in the atmospheric boundary layer. On the centreline
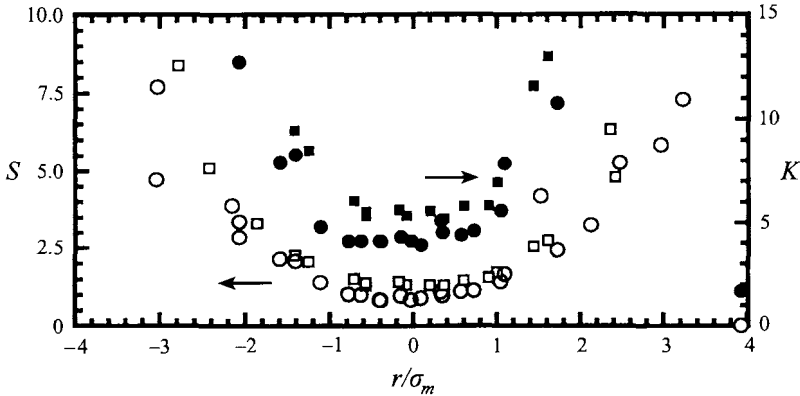
FIGURE 9. Profiles of skewness and kurtosis of mixture fraction at $x/M = 7$ and 17: open symbols, S; full symbols, K. Symbol shapes as in figure 5.

he obtains average values of 1.3 and 4.4, respectively, although there is considerable scatter in the data. The values of S and K from the present experiment at $x/M = 7$ and 17 bracket the average centreline values obtained by Sawford (1987) whose plume was released at a height of 0.5 m and measured 25 m down wind at a height of 0.8 m.

For self-similarity the normalized moments $\overline{f'}(x,r)/\overline{F}(x,r)$ and $\overline{f''}(x,r)/f'''(x,r)$ should be constant. However, the second normalized moment is found to be a weak function of axial distance ($f'_c/\overline{F} \propto (x/M)^{-0.32}$). Figure 8($b$) confirms this axial dependence by showing the centreline region in detail. Close examination of the centreline region of figure 9 shows that from $x/M = 7$ to 17, S drops from about 1.4 to 1.0 and K from 5.5 to 4.2 although there is some scatter of the points. All measurements have been made in the initial region of the decay of the turbulence ($x/M \leqslant 100$) and so self-similarity would not be expected (Hinze 1975, chapter 3). The data do, however, collapse quite well using σ_m as the cross-stream normalizing variable.

3.3. *Reactive species fields*

We shall now present the reactive scalar statistics which have not been measured in reactive plumes at the present resolution by others. As noted in §1 the reactive scalars are passive and have no effect on the fluid mechanics. From the conserved scalar statistics it is possible to calculate limiting cases for the reactive scalars. The limiting cases are important for the theoretical study of turbulent reacting flows and for validation of models. We consider three such limiting cases here: the frozen, equilibrium and reaction-dominated limits (Bilger *et al.* 1991). Each limit is a function of the mixture fraction and can readily be calculated from the conserved scalar data of §3.2. A brief explanation of the assumptions on which each limit is based will now be given. For full details the reader is referred to Bilger *et al.* (1991).

The Damköhler number is defined as

$$N_D \equiv \frac{kM\Gamma_{O_3,2}}{\overline{U}}. \tag{9}$$

It represents the ratio of the timescales of turbulence and chemical reaction. The value of N_D for all reactive experiments is approximately 0.24. The frozen limit ($N_D \rightarrow 0$) is the reactant concentration that would result by mixing without chemical reaction,

and is

$$\Gamma_{NO}^0 = F\Gamma_{NO,1}, \qquad \Gamma_{O_3}^0 = (1-F)\Gamma_{O_3,2}. \tag{10}$$

The equilibrium limit ($N_D \to \infty$) is the reactant concentration that would occur if the chemical reaction rate were infinite. The reaction rate in this case is mixing-limited and the reactant concentrations are

$$\Gamma_{NO}^e = (\Gamma_{NO,1}+\Gamma_{O_3,2})(F-F_s)H(F-F_s), \qquad \Gamma_{O_3}^e = (\Gamma_{NO,1}+\Gamma_{O_3,2})(F_s-F)H(F_s-F) \tag{11}$$

where $H(z)$ is the Heaviside unit step function with value zero for $z < 0$ and value unity for $z > 0$ and F_s is the stoichiometric mixture fraction. The latter is the mixture fraction at which both reactant concentrations are equal and is therefore obtained by setting $\Gamma_{NO} = \Gamma_{O_3}$ in (2).

The reaction-dominated limit, Γ_i^{rd}, assumes instantaneous mixing at $x = 0$ followed by reaction for the mean convection time from the point source, $x/\bar{U}$. It is valid when the smallest characteristic timescale of mixing is much greater than the characteristic timescale of the chemical reaction. The reactant concentration obeys

$$\frac{\partial \Gamma_i^{rd}}{\partial t} = w_i, \qquad \Gamma_i^{rd}(t=0) = \begin{cases} \Gamma_{NO,1} \\ \Gamma_{O_3,2} \end{cases} \tag{12}$$

and the solution of (12) is a lower bound on Γ_i^{rd} for any chemistry rate. The three limits discussed above bracket reactant concentrations as follows: $\Gamma_i^e \leqslant \Gamma_i^{rd} \leqslant \Gamma_i \leqslant \Gamma_i^0$. If this constraint is violated it can only be explained by differential diffusion or experimental error. There is no such constraint on variances, covariances, p.d.f.s and turbulent scalar fluxes.

The mean reaction rate is normalized by the ambient chemical timescale as follows (note that $\bar{w}_{NO} = \bar{w}_{O_3}$):

$$\hat{\bar{w}} = \frac{-\bar{w}_{NO}}{k\Gamma_{O_3,2}^2} = \frac{\overline{\Gamma_{NO}\Gamma_{O_3}}}{\Gamma_{O_3,2}^2} \tag{13}$$

and has the normalized frozen flow limit

$$\hat{\bar{w}}^0 = \frac{\Gamma_{NO,1}}{\Gamma_{O_3,2}} \left\{ \bar{F}(1-\bar{F}) - f'^2 \right\} \tag{14}$$

which can be simplified in plumes by noting that $\bar{F} \ll 1$ and $f'^2 \ll \bar{F}$ to

$$\hat{\bar{w}}^0 \approx \frac{\Gamma_{NO,1}}{\Gamma_{O_3,2}} \frac{1}{\bar{F}}. \tag{15}$$

The normalized equilibrium limit is (Bilger et al. 1991)

$$\hat{\bar{w}}^e = \left\{ \frac{1}{2} M \frac{\overline{\chi_s}}{\bar{U}} + \frac{\widehat{\nabla \bar{F}} \cdot \widehat{\nabla \bar{F}}}{Pe} \right\} \frac{p_F(F_s;x)}{N_D F_s} \tag{16}$$

where $\overline{\chi_s}$ is the conditional expectation of the scalar dissipation ($\chi \equiv 2\mathscr{D}\nabla f \cdot \nabla f$) for $F = F_s$, Pe is the Péclet number defined as $\bar{U}M/\mathscr{D}_{conserved\,scalar}$, $p_F(F;x)$ is the probability density function of F defined such that $p_F(F;x)dF$ is the probability that F lies between F and $F+dF$ at x, the gradients in $\bar{F}$, $\widehat{\nabla F}$, are non-dimensionalized by M and N_D. It can be shown (Bilger et al. 1991) that the mean reaction rate, $\bar{w}$ must lie between its respective frozen and equilibrium values. This experiment was designed to measure the statistics of the reactive scalars NO and O_3. The product, NO_2, was not measured and no results for it are presented. However, it is possible to find its statistics from the results presented here using $\Gamma_{NO_2} = \Gamma_{NO}^0 - \Gamma_{NO} = \Gamma_{O_3}^0 - \Gamma_{O_3}$.
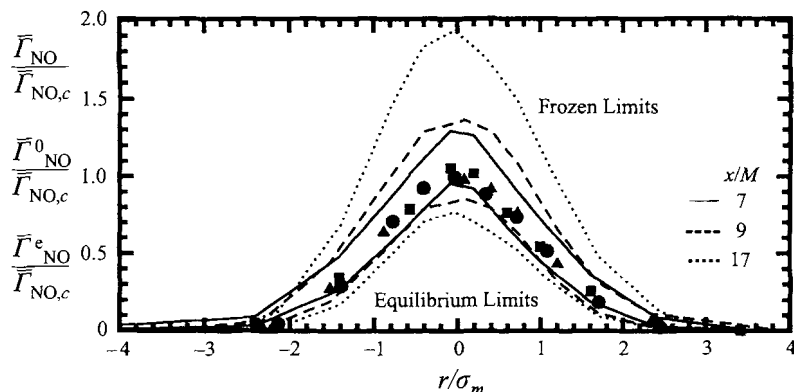
FIGURE 10. Mean NO concentration with frozen and equilibrium limits at $x/M = 7$, 9 and 17 with normalization of all profiles at each axial location by measured mean NO centreline concentration at that location. Symbols as in figure 5.
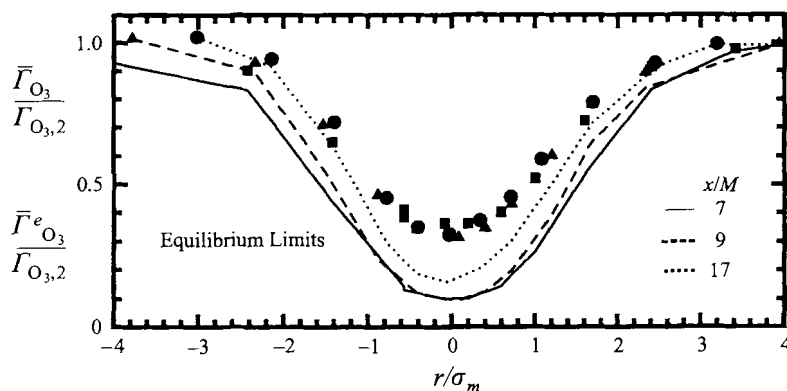

FIGURE 11. Mean O_3 concentration at $x/M = 7$, 9 and 17 normalized by unmixed O_3 concentration with frozen and equilibrium limits. Symbols as in figure 5.

Figure 10 shows profiles of mean NO concentration, $\overline{\Gamma}_{NO}$, with frozen and equilibrium limits all normalized by $\overline{\Gamma}_{NO,c}$ at $x/M = 7$, 9 and 17. The experimental results are bracketed by the limits that would be expected from conserved scalar theory. The profile of $\overline{\Gamma}_{NO}$ is close to Gaussian (not shown). Figure 11 shows profiles of mean O_3 concentration, $\overline{\Gamma}_{O_3}$, at $x/M = 7$, 9 and 17 normalized by $\Gamma_{O_3,2}$, the background concentration of O_3. The latter varied slightly between experiments because the ozone generator used was not able to produce a repeatable concentration from one experiment to another but the value during each experiment was constant. Table 1 shows values of $\Gamma_{O_3,2}$, which are close to 1 p.p.m. for all reactive experiments. $\overline{\Gamma}_{O_3}$ profiles collapse quite well using this method of normalization. Equilibrium limits are shown in figure 11 but frozen limits have been omitted for simplicity as they have an almost constant value near 1.0. There is a trend with increasing axial distance for $\overline{\Gamma}_{NO}$ and $\overline{\Gamma}_{O_3}$ at all radial locations to move relatively closer (in between frozen and equilibrium limits) to their respective equilibrium limits.

Only a few reactive plume results are reported in the literature. Useful comparisons to the present results can be made with the work of Builtjes (1993) who used a wind tunnel boundary layer and Ibrahim (1987) who used a point source of NO released into the wake of two opposed flows of O_3. Builtjes reports profiles of reactants parallel
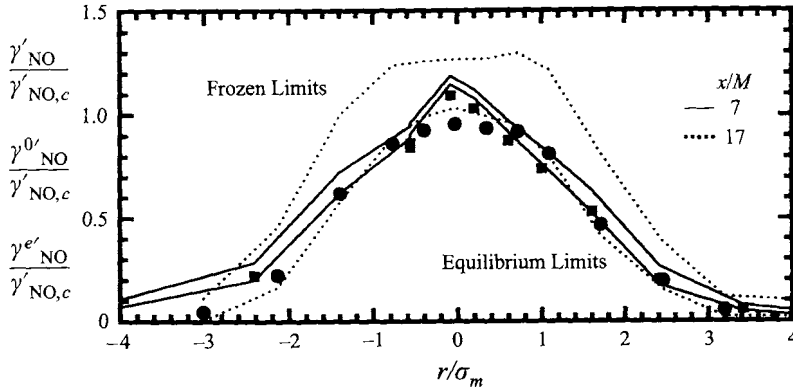
FIGURE 12. R.m.s. of NO concentration fluctuation at $x/M = 7$ and 17 normalized by centreline concentration with frozen and equilibrium limits. Symbols as in figure 5.
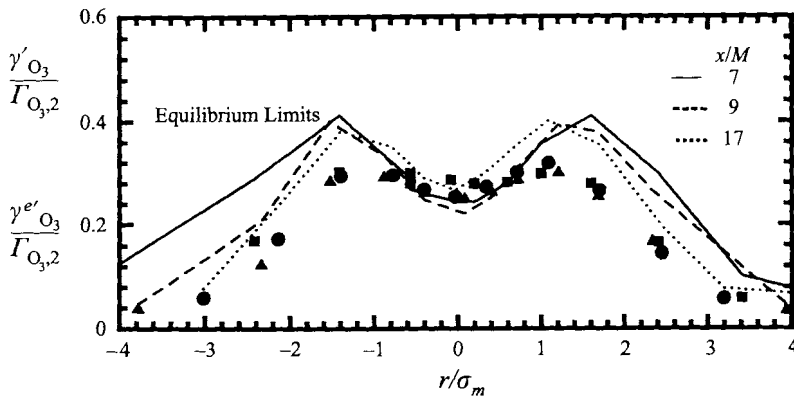

FIGURE 13. R.m.s. of O_3 concentration fluctuation at $x/M = 7$, 9 and 17 normalized by unmixed O_3 concentration with frozen and equilibrium limits. Symbols as in figure 5.

to the boundary-layer surface and on the centreline in a streamwise direction. The results show quite a lot of scatter because the experimental equipment could only reproduce measurements within 15% for O_3 and 30% for NO. The transverse mean reactant profiles are approximately Gaussian as in the present experiment and show similar features. The results of Ibrahim also show a lot of scatter. Radial profiles of the reactant means are approximately Gaussian. Probability density functions of the conserved scalar on the centreline show the presence of significant amounts of unmixed ambient fluid and the conserved and reactive scalar profiles do not reach 0 at the walls of the reaction chamber. This indicates that the mixing field is quite different to the present experiment and further comparison does not seem possible.

Figure 12 shows profiles of the r.m.s. NO concentration, γ'_{NO}, normalized by $\gamma'_{NO,c}$, at $x/M = 7$ and 17 with frozen and equilibrium limits. Unlike the mean values there is no theoretical constraint requiring r.m.s. values to fall between the frozen and equilibrium limits. In general γ'_{NO} lies at or below the equilibrium limit.

Figure 13 shows profiles of the r.m.s. O_3 concentration normalized in the same way as that for $\overline{\Gamma}_{O_3}$, $\gamma'_{O_3}/\Gamma_{O_3,2}$ at $x/M = 7$, 9 and 17. Equilibrium limits are shown but the frozen limits which are close to 0 are omitted for clarity. Like the results for γ'_{NO}, those for γ'_{O_3} lie close to their equilibrium limit, and similarly do at times lie
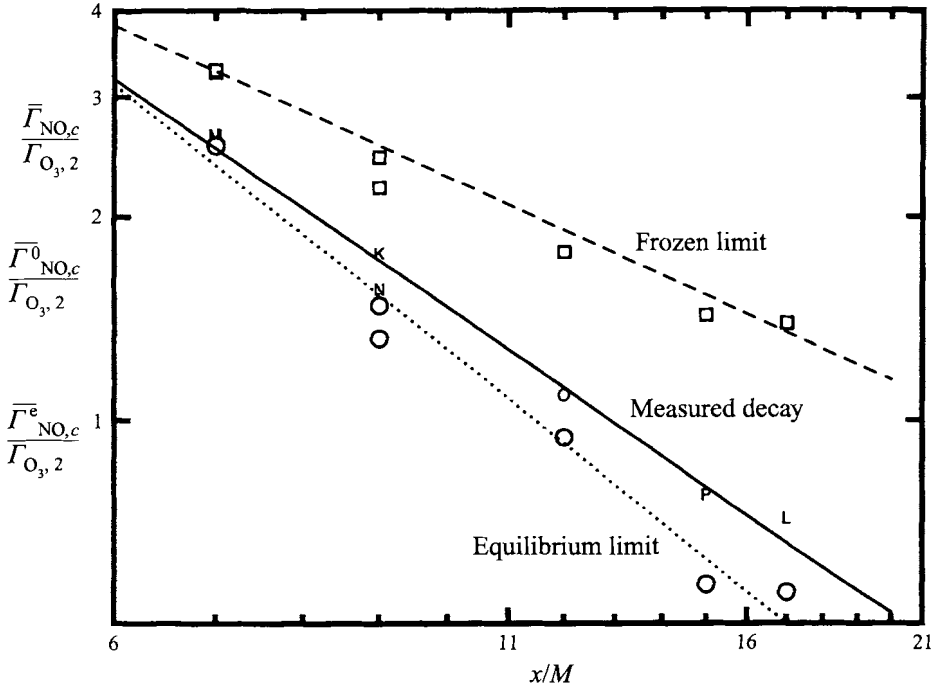
FIGURE 14. Axial decay of the centreline NO mean concentration normalized by unmixed O_3 concentration with frozen and equilibrium limits. The decay laws (17) are also shown. Symbols: upper case letters as in table 1, measured mean concentration; $\square$, frozen limit; $\circ$, equilibrium limit.

outside the bound of frozen and equilibrium limits. For the plume reactant (NO) the r.m.s. equilibrium limit can be seen from figure 12 to be below the r.m.s. frozen limit, indicating that the effect of reaction is to reduce the fluctuations. For the ambient reactant (O_3) the r.m.s. limits shown in figure 13 are the other way around indicating that the effect of reaction is to increase the fluctuations. When the reactant r.m.s. values and their respective limits are compared with the scalar mixing layer data of Bilger *et al.* (1991) it is found that the plume reactant has its limits placed in the same way as the reactant not in excess, i.e. the frozen limit is above the equilibrium limit. On the other hand the ambient reactant behaves as the reactant in excess and has its equilibrium limit above its frozen limit. The dip on the centreline of the O_3 r.m.s. profiles indicates that the ambient reactant is showing a tendency here not to be the reactant in excess. This is because mixing of the ambient reactant into the plume has not been sufficient on the centreline for O_3 to continue to be as abundant as it is off the centreline. The equilibrium limits for the O_3 r.m.s., which are a function of the mixture fraction only, also show this dip confirming that it is related to the mixing process.

The axial profile of normalized centreline NO mean and r.m.s., $\overline{\Gamma}_{NO,c}/\Gamma_{O_3,2}$ and $\gamma'_{NO,c}/\overline{\Gamma}_{NO,c}$ can be found in figures 14 and 15, respectively. Frozen and equilibrium limits with the same normalization are also shown. The empirical decay laws for the centreline NO mean and r.m.s with normalization as in figures 14 and 15 were found to be

$$\frac{\overline{\Gamma}_{NO,c}}{\Gamma_{O_3,2}} = K_{\Gamma_{NO}}(x/M)^{-1.51}, \qquad \frac{\gamma'_{NO,c}}{\overline{\Gamma}_{NO,c}} = K_{\gamma_{NO}}(x/M)^{0.031}. \tag{17}$$
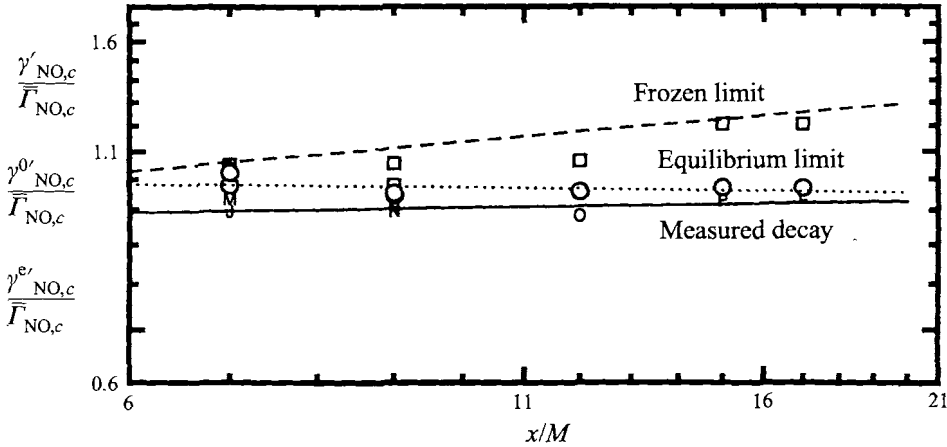
FIGURE 15. Axial decay of the centreline NO r.m.s. concentration normalized by NO mean centreline concentration. The decay laws (17) are also shown. Symbols: upper case letters as in table 1, measured r.m.s. concentration; □, frozen limit; ○, equilibrium limit.

A virtual origin was not needed and constants $K_{\Gamma_{NO}} = 47.43$ and $K_{\gamma_{NO}} = 0.843$ gave the best fit for this data. Decay exponents for centreline NO mean and r.m.s. frozen limits are $m = -1$ and -0.19, respectively, and that for equilibrium limits are -1.76 and -0.025, respectively. The decay exponent for the normalized r.m.s centreline concentration of NO is 0.031, which indicates that the NO r.m.s. intensity (i.e. r.m.s./mean) is virtually constant. The result is not surprising when it is noted that the frozen and particularly the equilibrium limits are also weak functions of axial position. It can be observed from figure 14 that there is no greater scatter for mean NO decay than that for the fitted decay lines for the mixture fraction derived from non-reactive and reactive experiments in figure 6. Further, the fit of the lines in both cases is quite good. This indicates that the effect of the chemical reaction on the reactant decay is constant in the axial region of measurement. This conclusion is confirmed by observing that the centreline mean equilibrium limit also decays at a constant rate.

Figure 16 shows profiles of skewness and kurtosis of NO concentration normalized by reactant r.m.s. values in the same way as that for the mixture fraction. As expected, NO, being a reactive scalar, has S and K which both depart from Gaussian values more than those for the mixture fraction. Near the centreline the profiles from different axial locations have collapsed better than that for the mixture fraction. This may be because the occurrence of low-probability, high-concentration fluid parcels containing NO, which contribute to non-Gaussian behaviour, is reduced under reactive conditions.

Figure 17 shows profiles of skewness and kurtosis of O_3 concentration normalized in the same way as that for the mixture fraction. As found for the S and K of NO, those for O_3 show better collapse than those for the mixture fraction. The K of O_3 has a peak on the centreline. The peak is related to the mixing process because the equilibrium values of K for O_3 (not shown) also have a peak.

3.4. Probability density functions

The p.d.f. of a conserved scalar (in this case mixture fraction) gives a complete description of the state of mixing of two fluids. It also gives information about the proportion of unmixed fluid present (scalar intermittency). Measured p.d.f.s of the
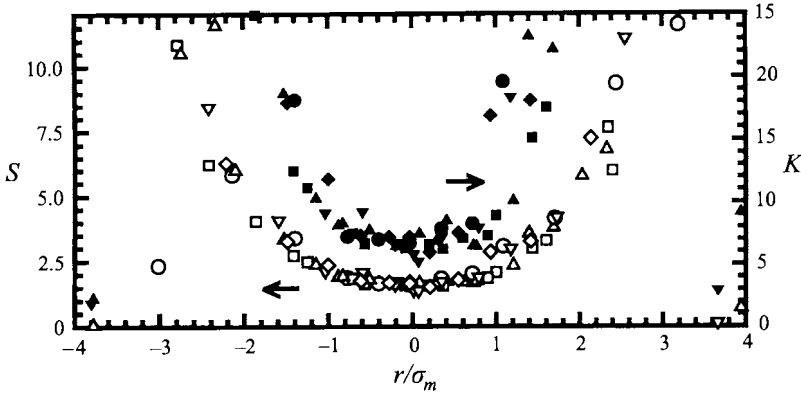
FIGURE 16. Skewness and kurtosis of NO concentration at $x/M = 7, 9, 12, 15$ and 17: open symbols, S; full symbols, K. Symbol shapes as in figure 5.
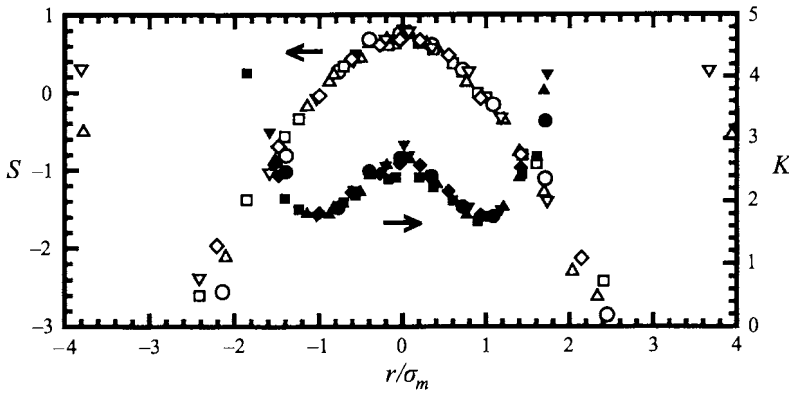

FIGURE 17. Skewness and kurtosis of O_3 concentration at $x/M = 7, 9, 12, 15$ and 17: open symbols, S; full symbols, K. Symbol shapes as in figure 5.

reactive scalars will be compared with frozen and equilibrium limits derived from the p.d.f. of the mixture fraction using conserved scalar theory.

Figure 18(a,b) shows NO probability density functions at $x/M = 17$ near to and away from the centreline at $r/\sigma_m = -0.033$ and 1.09, respectively. For presentation on the figures Γ_{NO}, Γ_{NO}^0 and Γ_{NO}^e are normalized by $\Gamma_{NO,c}^0$, the mean frozen limit centreline NO concentration, and denoted as z. Frozen and equilibrium limits were calculated using (10) and (11) as was done by Bilger *et al.* (1991). Figure 18(c,d) shows O_3 p.d.f.s normalized by $\Gamma_{O_3,2}$ with equilibrium limits prepared in the same way as that for NO. The frozen limit is not shown since it is close to a δ-function at unity. Because the reaction between NO and O_3 is a one-for-one reaction, the area under the p.d.f. equilibrium limit of one of the reactants (excluding δ-functions) will be the δ-function at $z = 0$ for the equilibrium limit of the other reactant. This is seen on the centreline NO p.d.f. equilibrium limit (figure 18a) where the area (excluding δ-functions) is 0.6 which corresponds to a centreline O_3 p.d.f. equilibrium-limit δ-function (figure 18c) of strength 0.6. The latter indicates that on the centreline NO is in excess. The situation is slightly more complicated off the centreline because unmixed fluid is present. This is represented as a δ-function of strength 0.15 at $z = 0$ and 1 for the NO (figure 18b) and O_3 (figure 18d) p.d.f. equilibrium limits, respectively. In addition to these scalar-intermittency δ-functions which occur off the
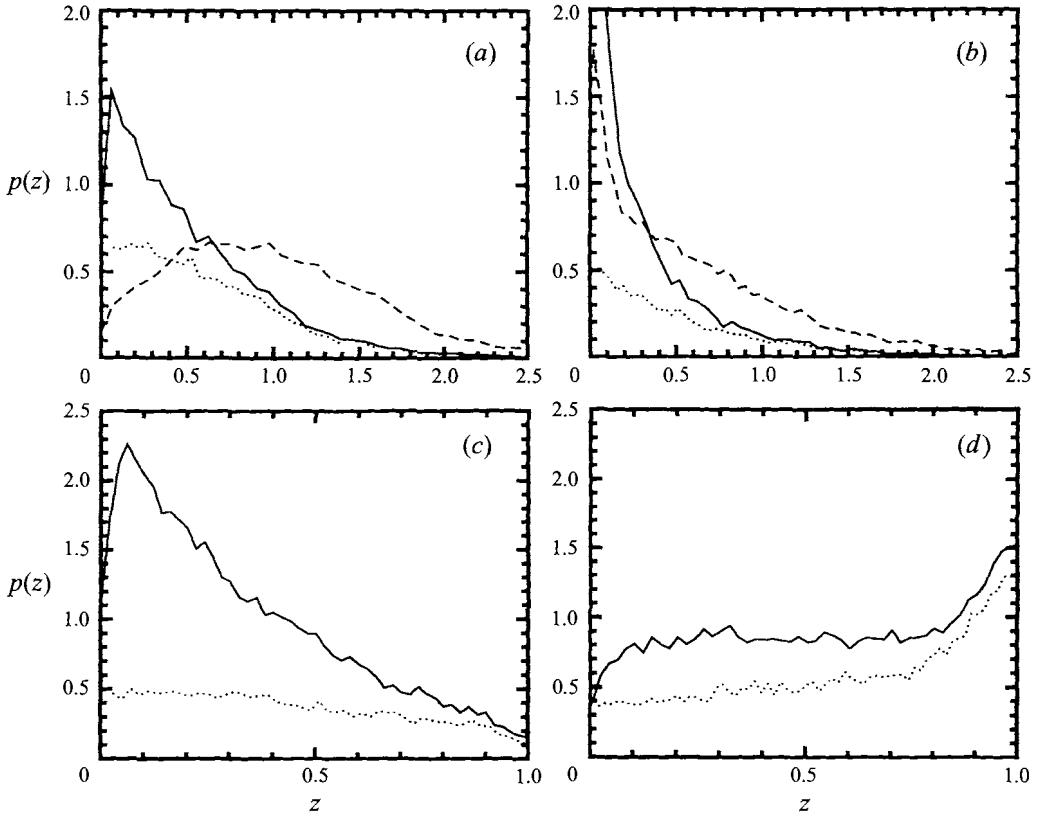
FIGURE 18. Probability density functions of reactants with frozen and equilibrium limits derived from (10) and (11), respectively, at $x/M = 17$. (a) NO, $r/\sigma_m = -0.033$; (b) NO, $r/\sigma_m = 1.09$; (c) O_3, $r/\sigma_m = -0.033$; (d) O_3, $r/\sigma_m = 1.09$. The full curve is the measured reactant p.d.f., the dashed curve is the frozen limit and the dotted curve is the equilibrium limit.

centreline others exist as a result of fully reacted fluid. The NO p.d.f. equilibrium limit (figure 18d) has an area (excluding δ-functions) of 0.25 which corresponds to an O_3 p.d.f. equilibrium-limit δ-function of strength 0.25 at $z = 0$. Excluding scalar-intermittency δ-functions, at finite Damköhler number there is no direct evidence of these δ-functions.

The mixture fraction is not shown on a separate figure because it is the same as the frozen limit for NO but with different normalization. It can be obtained from figure 18(a,b), where $z = \Gamma_{NO}/\Gamma^0_{NO,c}$, by the relation $p_F(F) = \Gamma_{NO,1}/\Gamma^0_{NO,c}p_z(z\Gamma^0_{NO,c}/\Gamma_{NO,1})$. Off the centreline the measured NO frozen limit (mixture fraction) has a δ-function at zero mixture fraction associated with unmixed fluid. The δ-function is smeared by noise. On the centreline it can be seen from the NO frozen-limit p.d.f. that there is very little unmixed ambient fluid present. The results of Gad-el-Hak & Morton (1979) in the range $x/M = 10$ to 45, using smoke in air, show no unmixed fluid present between $r/\sigma_m = 0$ and $r/\sigma_m = 1$, while Nakamura et al. (1987) in water in the range $x/M = 13.25$ to 40, find that concentration signals are quite intermittent even on the centreline. The data of Gad-el-Hak & Morton (1979) may show a larger region where unmixed fluid is absent around the centreline because of their use of a relatively large point source of diameter $d_{ps}/M = \frac{1}{2}$, whereas we have used $d_{ps}/M = \frac{1}{10}$. The increased intermittency on the centreline found by Nakamura et al. (1987) may
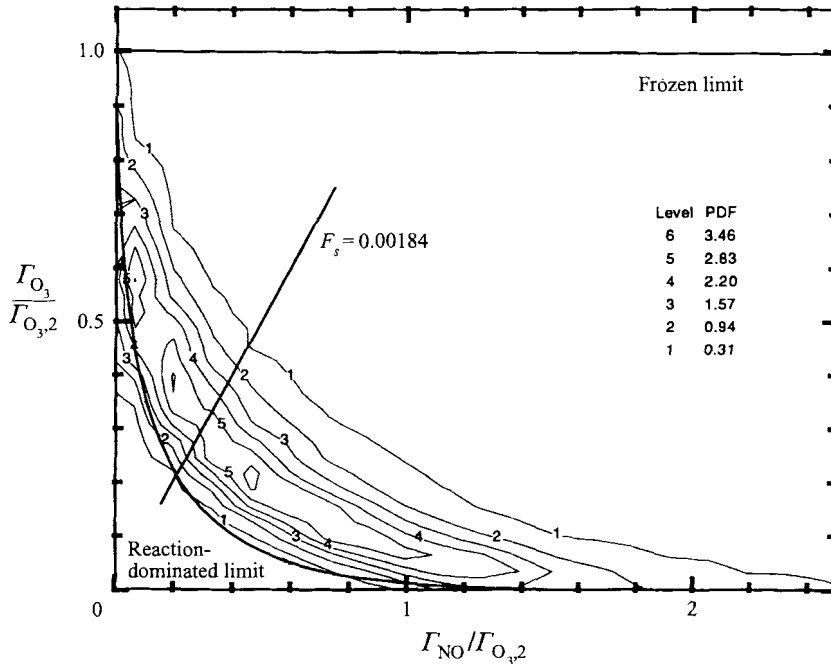
FIGURE 19. Joint probability density function of the two reactants with the reaction-dominated limit at $x/M = 17$ and $r/\sigma_m = -0.033$.

be the result of Schmidt number ($= \nu/\mathcal{D}$) effects because their experiment was in water. Further detailed comparison between these two results and the present results is not possible because of differences in relative size, placement and velocity of the point sources, measurement thresholds of instruments and properties of the fluids.

Turning now to the behaviour of the reactants it can be observed that off centreline in figure 18(b) the NO p.d.f. is behaving as that of a reactant not in excess. Higher concentrations are close to the equilibrium limit and lower concentrations form a δ-function because they result from reacted-out fluid. The corresponding off-centreline p.d.f. for O_3, shown in figure 18(d), is typical of a reactant in excess. The measured p.d.f. has a δ-function over the unmixed O_3 concentration showing that little or no O_3 has reacted there and the reactant p.d.f. is well above its equilibrium limit. On the centreline the measured NO p.d.f. of figure 18(a) is still generally typical of that of a reactant not in excess, but not to the extent of that off the centreline. The O_3 p.d.f. on the centreline, shown in figure 18(c), is more typical of that of a reactant not in excess, which is in contrast to its behaviour off the centreline shown in figure 18(d). This behaviour is consistent with that of the O_3 r.m.s. profiles shown in figure 13 where the presence of a dip on the centreline of the measured and equilibrium limit was caused by insufficient O_3 being brought to the centreline by the mixing process. Apparently, on the centreline there is not sufficient O_3 available for its behaviour to remain fully that of a reactant in excess. The behaviour of the p.d.f.s of NO and O_3 to be that of reactants not in excess and in excess, respectively, is consistent with that of the reactants in the scalar mixing layer of Bilger *et al.* (1991), which has been discussed above in relation to the reactant r.m.s. values. In brief the reactant on the side from which it does not come behaves in the same way as the plume (NO)
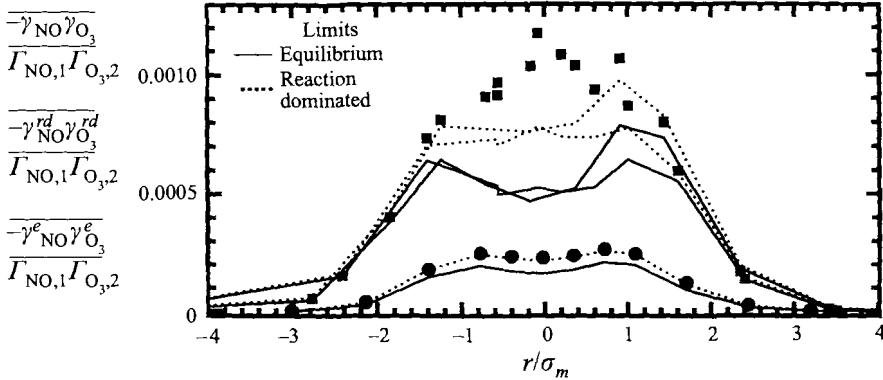
FIGURE 20. Reactant covariance normalized by inlet concentrations at $x/M = 7, 17$ with equilibrium and reaction-dominated limits. Symbol shapes as in figure 5.

reactant while the reactant on the side from which it does come behaves in the same way as the ambient reactant (O_3).

The joint p.d.f. of Γ_{NO} and Γ_{O_3} is shown in figure 19 on the centreline at $x/M = 17$. Under frozen conditions the p.d.f. lies on the line $\Gamma_{O_3}/\Gamma_{O_3,2} = 1 - (\Gamma_{O_3,2}/\Gamma_{NO,1})(\Gamma_{NO}/\Gamma_{O_3,2})$. At the equilibrium limit the deficient reactant is zero and so the p.d.f. lies along the axes. The reaction-dominated limit (Bilger et al. 1991; Kerstein 1992; Mell et al. 1994), which assumes instantaneous mixing at $x = 0$ followed by reaction for the mean time of convection from the point source, is also shown on the p.d.f. The limit has a hyperbolic shape and is a lower bound on the reactants for any given mixture fraction. This is in contrast to the results of Bilger et al. (1991) who, somewhat unexpectedly, found the reaction-dominated limit approximately followed the median reactant concentration. Lines of constant mixture fraction on figure 19 are diagonals parallel to the line shown for constant stoichiometric mixture fraction, which is $\Gamma_{O_3}/\Gamma_{O_3,2} = \Gamma_{NO}/\Gamma_{O_3,2}$.

3.5. Species covariance and reaction rate closure

Measurements of joint statistics of reactive scalars in turbulent reactive plumes are difficult to make. Results at the present resolution are not found elsewhere in the literature. Of particular interest here is the mean reaction rate because of the need to find a closure for this term when modelling turbulent reacting flows. It is a non-linear function which has been modelled in many ways as discussed in §1. Some of these closures will be compared with the reaction rate measured in the present plume. The reaction-dominated limit is shown on the joint p.d.f. of Γ_{NO} and Γ_{O_3} and is discussed in §3.4.

Figure 20 shows reactant covariance at $x/M = 7$ and 17, normalized by unmixed reactant concentrations, $\overline{\gamma_{NO}\gamma_{O_3}}/\Gamma_{NO,1}\Gamma_{O_3,2}$. The equilibrium and reaction-dominated limits are shown at both locations but the frozen limits are not shown because they are very small. Data lie at the equilibrium limit away from the centreline but are beyond the equilibrium limit on the centreline indicating that the effect of reaction has been to greatly increase the covariance. At $x/M = 7$ the equilibrium limit has a dip on the centreline but the data do not have a dip. The equilibrium limit is a function of the mixture fraction and so its dip must be related to the mixing process. At $x/M = 17$ the dip in the equilibrium limit is smaller but the data do follow it. The correlation coefficient $R_{NO,O_3} = \overline{\gamma_{NO}\gamma_{O_3}}/\gamma'_{NO}\gamma'_{O_3}$, is similar for all profiles, being
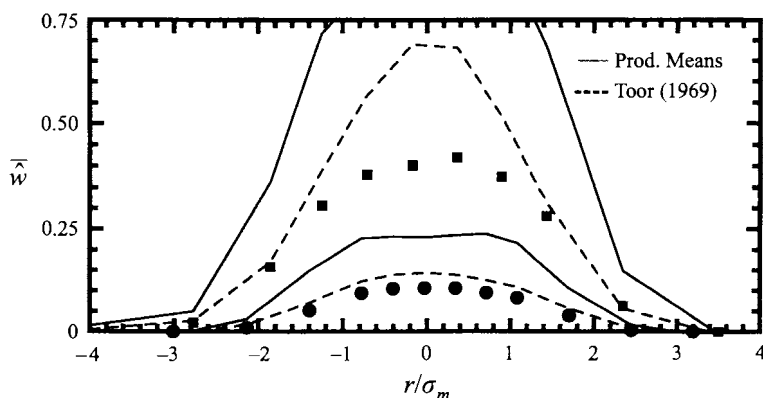
FIGURE 21. Mean reaction rate profiles normalized according to (13) at $x/M = 7$ and 17 with the closures of product means and Toor. Symbol shapes as in figure 5.

-0.77 on the centreline and rising to -0.82 at $r/\sigma_m = 1.8$. Beyond $r/\sigma_m = 3.0$ R_{NO,O_3} falls quickly to zero. R_{NO,O_3} lies between its frozen value of -1 and its equilibrium value of about -0.4 on the centreline and -0.59 at $r/\sigma_m = 1.8$. Bilger *et al.* (1991) find values of R_{NO,O_3} between -0.8 and -0.6 on the centreline of a reacting scalar mixing layer for N_D (defined in their experiment as $kM(\Gamma_{NO,1} + \Gamma_{O_3,2})/\overline{U}$) between 0.3 and 1.98 using a similar flow field to this experiment. Atmospheric measurements of R_{NO,O_3} have been found to lie between -0.4 and -0.8 and its value is critical in models of atmospheric chemistry (Vila-Guerau de Arellano, Talmon & Builtjes 1990).

The intensity of segregation, $\alpha = \overline{\gamma_{NO}\gamma_{O_3}}/\Gamma_{NO}\Gamma_{O_3}$, is qualitatively similar to R_{NO,O_3}, being -0.55 on the centreline and rising to -0.6 off the centreline. It is also bracketed by frozen and equilibrium values of about -0.005 and -1, respectively on the centreline. The similarity in the behaviour of α and R_{NO,O_3} is because the only difference in these two quantities is in their denominators, which contain reactant means and r.m.s. values, respectively. For a constant value of r/σ_m the ratios of r.m.s. to mean for NO and O_3 (i.e. γ'_{NO}/Γ_{NO} and $\gamma'_{O_3}/\Gamma_{O_3}$) are approximately constant at all axial measurement locations. For NO this can be seen in (17) and for O_3 it can be observed by comparing figures 11 and 13. An experiment conducted by Komori & Ueda (1984) gave positive values of α of up to 20 in a turbulent reacting plume similar to the one studied here. Theoretical difficulties for $\alpha > 0$ in a non-premixed reacting flow were pointed out by Bilger, Mudford & Atkinson (1985) because a positive value does not lie between the frozen and equilibrium limits. Komori *et al.* (1991) have more recently indicated a possible reason for the positive values of α. Their wind tunnel was not designed to homogeneously dilute O_3 with air to a scale less than the Kolmogorov scale so a truly non-premixed condition may not have been attained in the ambient O_3 coflow. Dependence of R_{NO,O_3} and α on variation in initial reactant concentration is to be investigated in further work.

Figure 21 shows the normalized mean reaction rate, $\widetilde{w}$, as given in (13) at $x/M = 7$ and 17. The frozen reaction rate, obtained from (14), is not shown since its value is beyond the scale for most of the range of r/σ_m, for example, on the centreline at $x/M = 7$ and 17, $\widetilde{w}^0 = 3.24$ and 1.34, respectively. The equilibrium reaction rate on the centreline can be obtained by using the simplifying assumptions that the second term in (16) is negligible and that $\overline{\chi}_s \approx \overline{\chi}$. The value of $\overline{\chi}$ used is that found from the mixture-fraction variance flux data using (19); and $\widetilde{w}^e$ can be calculated relatively
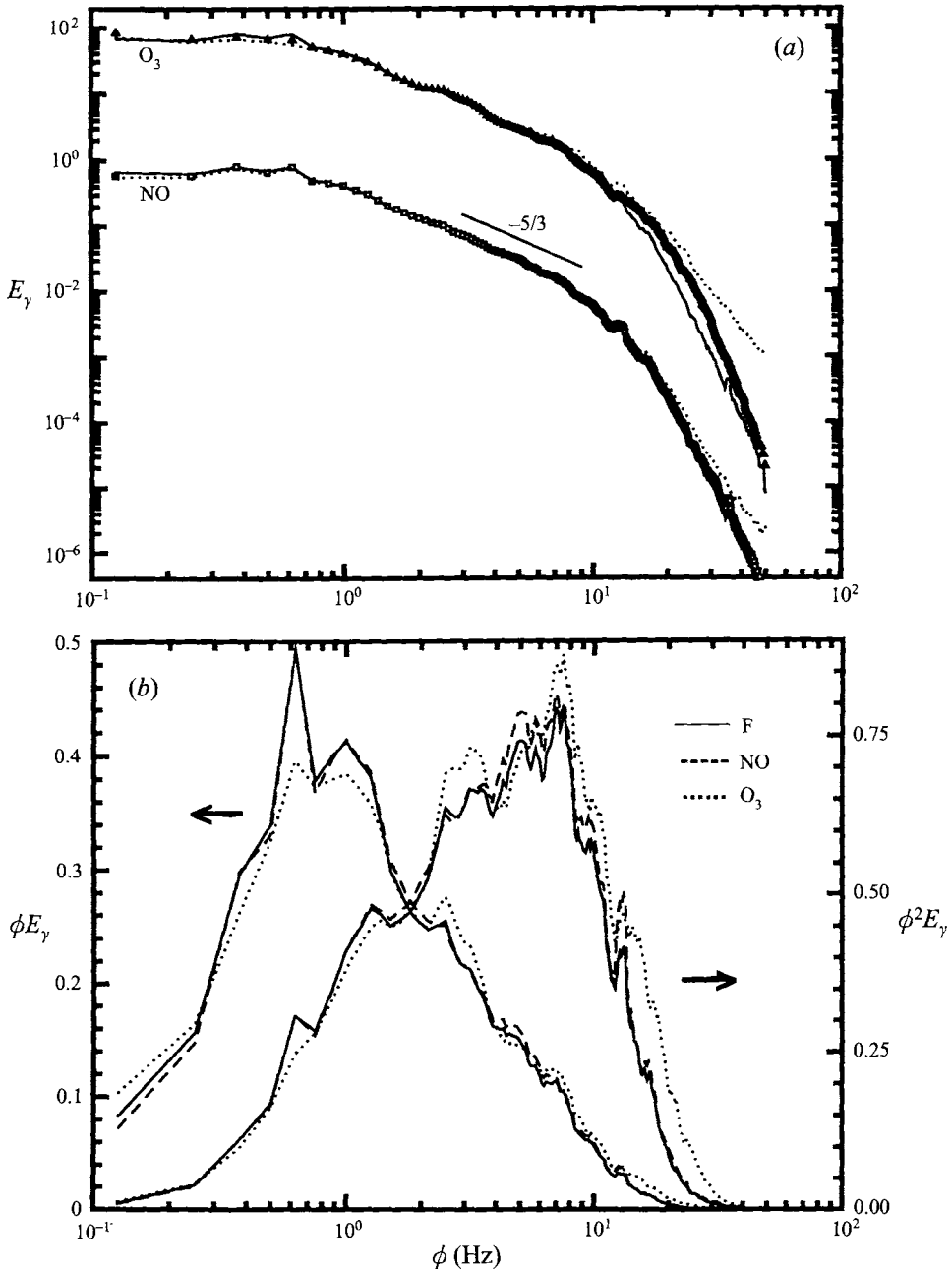
FIGURE 22 (a, b). For caption see facing page.

easily, and is found to be 0.30 and 0.10 at $x/M = 7$ and 17, respectively. When the frozen and equilibrium limits for $\bar{w}$ estimated above are compared with the data of figure 21 it is found that the measured data are bracketed by their limits as is predicted by conserved scalar theory. Further, the reaction rate is approaching its equilibrium limit with increased distance downstream which is in agreement with the trend for the mean values of the reactants and their covariance.

The simple product of means closure, which neglects the covariance $\overline{\gamma_{NO}\gamma_{O_3}}$, is
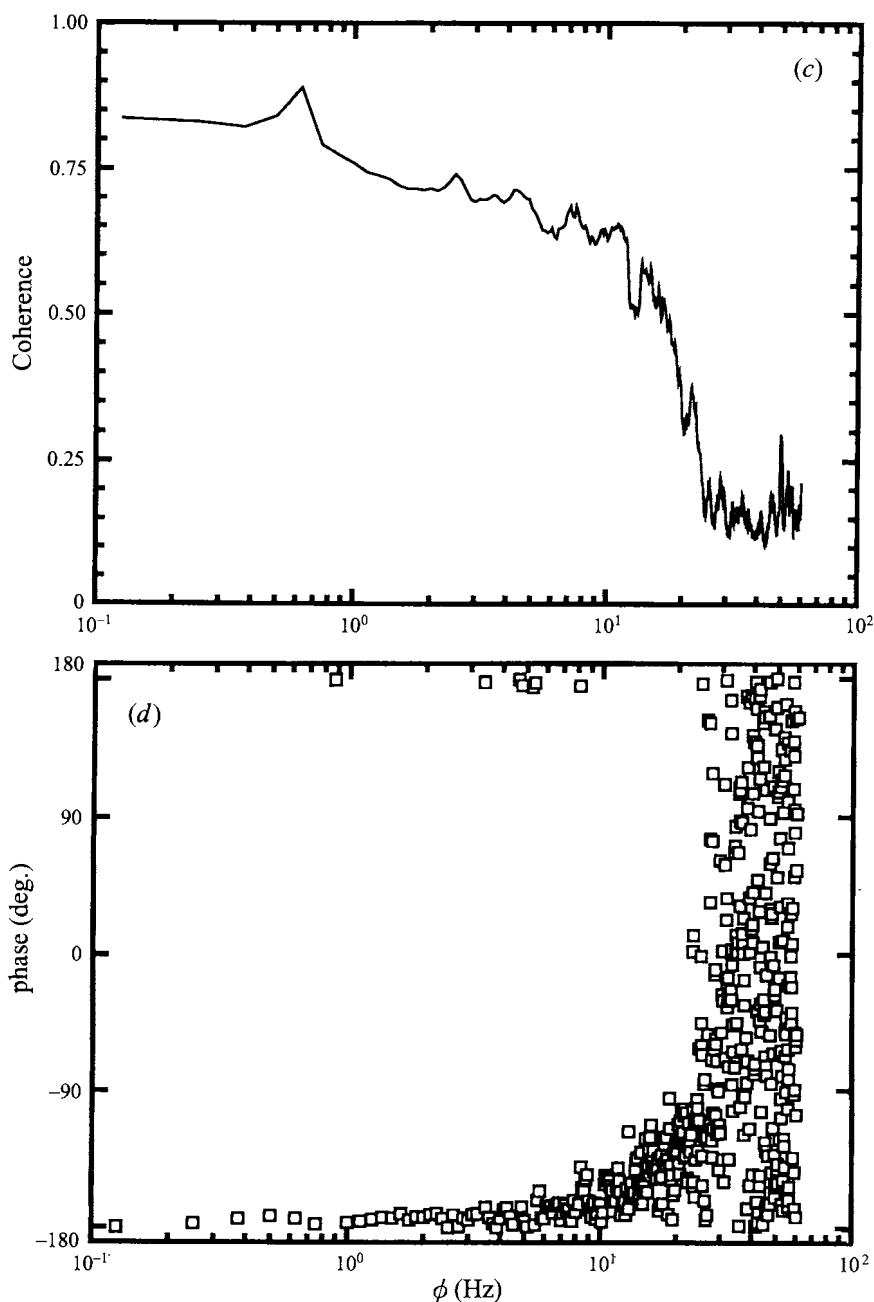
FIGURE 22. (*a*) Spectra for mixture fraction, NO and O_3 at $x/M = 17$ and $y/\sigma_m = -0.003$. The full curves are the mixture fraction (frozen limit for both reactants), symbols are the measured reactant spectra and the dotted curves are the equilibrium limits. Frozen, measured and equilibrium spectra for O_3 are shown two decades higher. A line of slope $-\frac{5}{3}$ is also shown. (*b*) Mixture fraction and reactant pre-multiplied and dissipation spectra; (*c*) coherence of cross-spectral density function between γ_{NO} and γ_{O_3}; (*d*) associated phase.

shown on figure 21. The agreement with the measured values is poor. The closure proposed by Toor (1969) is also shown. This closure simplifies the covariance $\overline{\gamma_{NO}\gamma_{O_3}}$ to its equilibrium value $\overline{\gamma^e_{NO}\gamma^e_{O_3}}$ (as shown in figure 20). The Toor closure overestimates the reaction rate considerably at $x/M = 7$ but is within 15% of the measured values at $x/M = 17$. Figure 20 shows that the measured values of covariance lie beyond the equilibrium limit but do approach the limit with increased axial distance. The Toor closure will always overestimate $\widehat{w}$ while the covariance lies beyond its equilibrium limit.

3.6. Spectra

Figure 22(a) shows spectra for mixture fraction and reactive scalar (including equilibrium limit) fluctuations close to the centreline at $x/M = 17$ and $r/\sigma_m = -0.033$. The spectrum for the mixture fraction represents frozen limits for both reactants. Frozen, measured and equilibrium spectra for O_3 have been moved up two decades. The power spectral density, $E_\gamma(\phi)$, has been normalized so that the area under the graph is unity. A line of slope $-\frac{5}{3}$ is shown in figure 22(a) indicating a region where an inertial subrange exists. The spectrum for the mixture fraction (frozen limit) and NO are virtually identical down to the cutoff frequency of 64 Hz. The spectrum of O_3 is slightly higher than that for the frozen limit below about 10 Hz. The spectrum of the O_3 equilibrium limit is noticeably higher than that for NO below 7 Hz. This difference in measured and equilibrium spectra of NO and O_3 is not due to a low signal level being dominated by noise because, here on the centreline, $\overline{\Gamma}_{O_3} = 0.307$ p.p.m. is lower than $\overline{\Gamma}_{NO} = 0.672$ p.p.m., yet away from the centreline, where $\overline{\Gamma}_{O_3}$ increases and $\overline{\Gamma}_{NO}$ decreases, the spectra demonstrate similar behaviour. It is possible that the high-frequency spectrum of O_3 contains contributions from residual fluctuations due to incomplete mixing with the air. However, the most likely explanation is that O_3 is behaving as a reactant in excess. A reactant in excess has its fluctuations increased by reaction. Its measured and equilibrium limit would be expected to be further above its frozen limit than that for NO, which is a reactant not in excess (deficient reactant).

The pre-multiplied and dissipation spectra of the mixture fraction and reactants at $x/M = 17$ and $r/\sigma_m = -0.033$ are shown in figure 22(b). The variance-bearing eddies peak at about 1 Hz which is the same frequency as the peak of the turbulent-energy-containing eddies. The peak of the mixture-fraction dissipation spectrum occurs at approximately 6 Hz. The Kolmogorov lengthscale, η, at this location in the experiment has previously been estimated to be about 2.7 mm which corresponds to a frequency of 185 Hz. The peak of the dissipation of the mixture fraction is occurring at about 30η. This agrees with the estimate of the maximum dissipation by Warhaft & Lumley (1978). It is thought that the maximum dissipation of the reactive scalars should occur at a frequency close to that of the conserved scalar, and this appears to be the case. The frequency response of the chemiluminescent analysers extends well into the region where dissipation is occurring.

Figures 22(c) and 22(d) show the coherence between Γ_{NO} and Γ_{O_3} and associated phase shift at $x/M = 17$ and $r/\sigma_m = -0.033$. These two figures show that the reactants still correlate with each other in the frequency range where maximum dissipation occurs. Beyond 20 Hz the coherence in figure 22(c) falls quickly and the phase in figure 22(d) becomes uncorrelated. This is in agreement with the coherence and phase of the reactants in the scalar mixing layer of Li et al. (1993). It is not possible to say whether this break at 20 Hz is due to the behaviour of the reactants or to instrument response. At these frequencies the signal amplitude is low so the

signal to noise ratio is poor. Beyond about 25 Hz the coherence drops to the level of noise but this will make no contribution to the local correlation coefficient because the phase shift is random in this region. The correlation coefficient at the sampling location for figure 22 is $R_{NO,O_3} = -0.77$. While it receives contributions from frequencies up to 20 Hz it can be seen from the reactant spectra in figure 22(a) that by 2 Hz the magnitude is down by a factor of 5. Thus nearly all the contributions to R_{NO,O_3} come from frequencies close to the energy-containing eddies around 1 Hz.

3.7. Fluxes

Turbulent transport is an important part of any modelling of turbulent reacting flow.

Figure 23(a) shows profiles of turbulent fluxes normalized by r.m.s. values to give the correlation coefficient, $\overline{vf}/(v'f')$, at all axial measuring locations. Comparison of the flux data with directly measured fluxes from other experiments is limited because few experiments make the necessary simultaneous measurement of scalars and velocities. The flux data of figure 23(a) are in qualitative agreement with those of Gad-el-Hak & Morton (1979) who measured fluxes in smoke plumes using laser-Doppler velocimeter techniques. Their point source was located at $x_0 = 0$. The maximum correlation coefficient they obtained was 0.35 which is consistent with the present results, although their centreline value does not return to zero. Owing to the disturbance effect of their method of introducing the smoke and the difficulty of obtaining concentration fluctuation measurements their results show considerable scatter which limits further comparison. Fluxes have also been measured by Komori & Ueda (1984) in a thermal plume at the same axial location from the grid as the present results ($x/M = 17$), though the point source was located at $x_0 = 0$ and had a larger diameter, $d_{ps}/M = \frac{1}{3}$ (the present experiment has $d_{ps}/M = \frac{1}{10}$). These results cannot be presented on figure 23(a) because σ_m is not given and the fluxes are normalized by the local mean values. When the present results are recalculated in this alternative form it is found that the general shape of the flux profile is similar: the peak occurs at approximately the same radial location but its magnitude, $\overline{vf}_{max}/\bar{U}\bar{F}_c = 0.0064$, is only approximately half of that found by Komori & Ueda (1984). Further comparison between their scalar transport and that of the present experiment is made later using the normalized turbulent diffusivity.

Turbulent fluxes of the reactants, NO and O_3, normalized by the local r.m.s. values to give the correlation coefficient are shown in figures 23(b) and 23(c), respectively at all axial measuring stations. Equilibrium limits, normalized by local measured r.m.s. values, are shown only at $x/M = 7$ and 17 for clarity. Frozen limits for NO (not shown) are the same as that for the mixture-fraction flux. Frozen limits for O_3 are not shown because they are close to zero. The mixture-fraction-flux correlation coefficient has a maximum magnitude of approximately 0.35 while that for NO is 0.3 and that for O_3 is 0.45. The measured correlation coefficients for the NO and O_3 fluxes are close to their equilibrium limits at all axial locations. The equilibrium limits for the plume (NO) fluxes are greater in magnitude than those for their respective frozen limits whereas those for the ambient (O_3) fluxes are reversed. This behaviour of the plume and ambient limits is the same as that noted for the limits of the reactant r.m.s. values of figures 12 and 13. It is also consistent with that observed in the reacting scalar mixing layer of Bilger *et al.* (1991) for reactants that are not in excess and in excess, respectively. These results indicate that in modelling reacting plumes the

(a)

$\dfrac{\overline{vf}}{v'f'}$

(b)

$\dfrac{\overline{v\gamma}_{NO}}{v'\gamma'_{NO}}$

$\dfrac{\overline{v\gamma^e}_{NO}}{v'\gamma'_{NO}}$

x/M
——— 7
········ 17

(c)

$\dfrac{\overline{v\gamma}_{O_3}}{v'\gamma'_{O_3}}$

x/M
——— 7
········ 17

$\dfrac{\overline{v\gamma^e}_{O_3}}{v'\gamma'_{O_3}}$
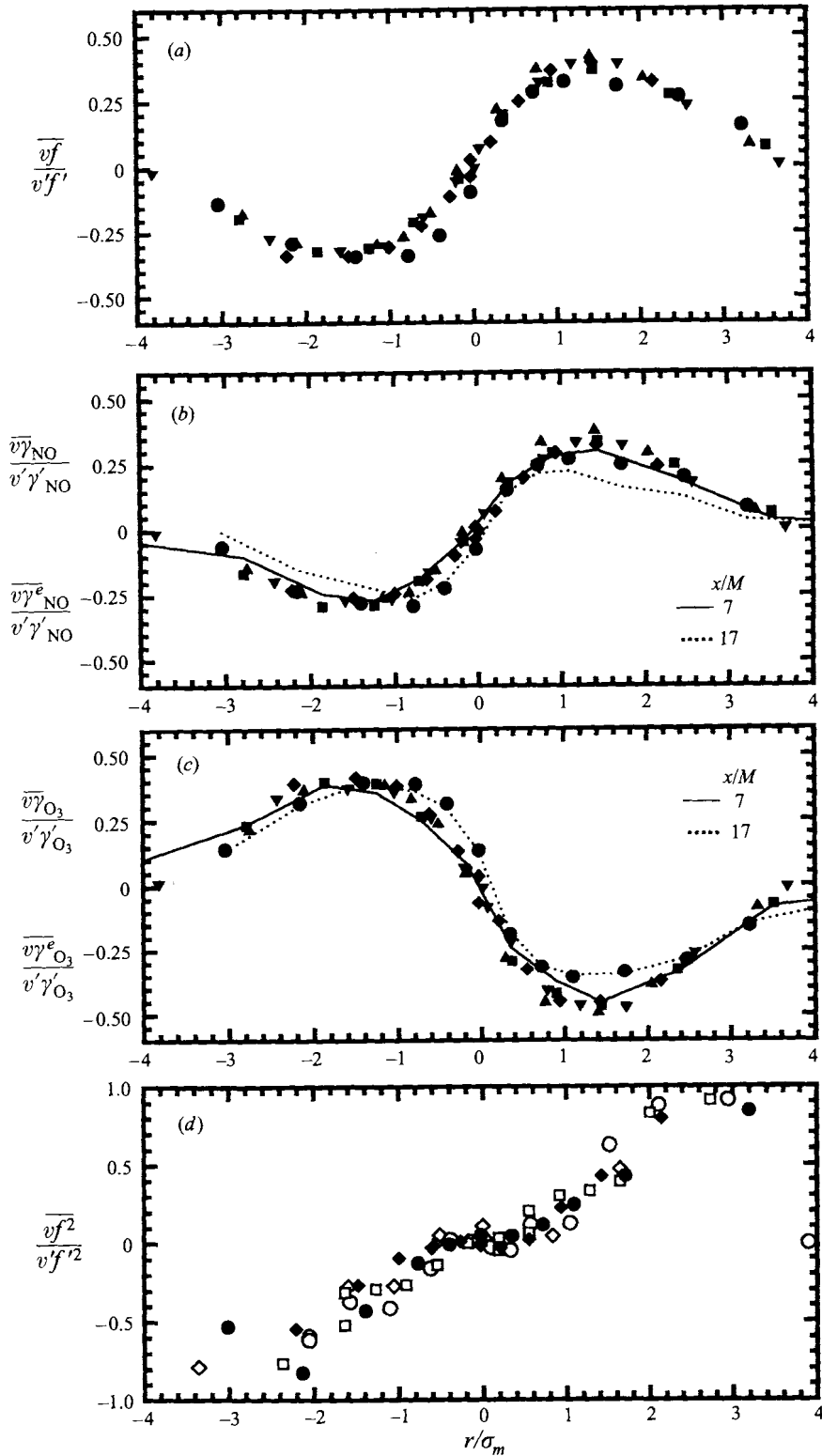
(d)

$\dfrac{\overline{vf^2}}{v'f'^2}$

r/σ_m

FIGURE 23. For caption see facing page.

plume reactant may possibly be determined simply from its equilibrium limit whereas this may not so for the ambient reactant.

Assuming high Reynolds numbers, negligible axial fluxes and equal diffusivities of reactants, the flux measurements were checked using the balance equation for the mixture fraction,

$$\overline{U}\frac{\partial \overline{\Gamma}}{\partial x} + 2\frac{\partial \overline{v\gamma}}{\partial r} = 0. \tag{18}$$

The second term in (18), the diffusion term, changes rapidly and it was difficult to determine accurately except on the centreline. At this location the imbalance of the terms was no more than 10% of the total magnitude of all terms.

Figure 23(d) shows profiles of the variance flux, $\overline{vf^2}$, normalized by the local r.m.s. values to give the triple correlation coefficient. The profiles collapse satisfactorily but with more scatter than that for $\overline{vf}$, which is to be expected for a third-order correlation.

An estimate of the mean scalar dissipation, $\overline{\chi}$, may be made from figure 23(d). The balance equation for the scalar variance can be simplified using the assumptions of (18) near the centreline to

$$\overline{U}\frac{\partial \overline{f^2}}{\partial x} + 2\frac{\partial \overline{vf^2}}{\partial r} + \overline{\chi} = 0. \tag{19}$$

Equation (19) is solved for $\overline{\chi}$. Because the radial gradient of $\overline{vf^2}$ changes very rapidly on the centreline the scatter in the points makes it very difficult to estimate the gradient accurately. The centreline gradient has therefore been estimated by first taking a representative gradient through a point on the linear part of the flux profile on figure 23(d). Actual gradients were then found by multiplying by f'^2, obtained from (4) and v', which is approximately constant in the radial and axial directions.

At $x/M = 15$ and 17 values of $\overline{\chi}$ were 8.5×10^{-7} s^{-1} and 5.3×10^{-7} s^{-1}, respectively. In order to compare these values of $\overline{\chi}$ with those obtained by other investigators the timescale ratio of kinetic energy dissipation to that of scalar dissipation, $a_\chi = (\overline{\chi}/f'^2)/(\epsilon/k_t)$, was calculated. At $x/M = 15$ and 17 values for a_χ of 1.8 and 2.1, respectively were found, while stations closer to the grid had lower values. The growth in a_χ could be because of changes in the way the plume is developing and/or because the simplifying assumptions of (19) break down. The values are, however, comparable with those found in other flows such as the thermal scalar mixing layer of Ma & Warhaft (1986) who find a value of 1.6 at high x/M or the value of 2 commonly used in modelling turbulent reacting flows. Gehrke & Bremhorst (1993) have estimated a_χ in air using a multi-bore jet block in which one jet is heated in the region $9 \leqslant x/M \leqslant 140$ and find values in the range 1.8 to 1.6. The configuration of their experiment is the closest to the present experiment known where dissipation estimates have been made. They used a Reynolds number close to that of the present experiment. Although they obtained a similar value of a_χ care should be taken in making a direct comparison because they used temperature as the passive scalar whereas we have used gas concentration. However, the difference between these two scalars is expected to be relatively small because the Prandtl ($= \nu/\alpha$) and Schmidt

FIGURE 23. Profiles of correlation coefficients obtained from turbulent fluxes normalized by r.m.s. values at $x/M = 7$, 9, 12, 15 and 17 unless stated otherwise. Symbols as in figure 5. (a) Mixture fraction. (b) NO with equilibrium limits at $x/M = 7$ and 17. (c) O$_3$ with equilibrium limits at $x/M = 7$ and 17. (d) Mixture fraction variance at $x/M = 7$, 15 and 17.

$(= \nu/\mathscr{D})$ numbers are approximately equal. Given the uncertainties in the estimation of a_χ from figure 23(d), its closeness to values found by Gehrke & Bremhorst (1993) in a point source, and other investigators in different types of flows, confirms the reliability of the measurement technique used.

4. Conclusions

Measurements in a turbulent reacting plume are made at a resolution not previously reported in the literature. The frequency response and spatial resolution of the chemiluminescent analysers used to measure the concentration fluctuations are found to be adequate to measure reactant higher moments, p.d.f.s, fluxes and spectra. Conserved scalar theory is used to deduce a conserved scalar from the reactive scalars. The conserved scalar data are internally consistent from source strength and conservation considerations. Conserved scalar data are compared with existing non-reacting plume data and found to be consistent with them where valid comparisons can be made. It is concluded that the assumptions of conserved scalar theory (including the equal diffusivity assumption) are basically valid for this flow and that the theory is a very useful framework for interpreting the data from turbulent reacting flows. The development of the plume is in the region relatively close to the grid and the decay of the normalized conserved scalar moments indicates that self-similarity has not yet been reached.

Data for the reactive scalars have been compared with frozen and equilibrium limits based on the conserved scalar theory. At the Damköhler number used (0.24) it has been found that the reactant moments are, in general, closer to the equilibrium limit than the frozen limit. The reactant statistics are bracketed by the limits where there is a theoretical requirement that this be so, i.e. in the case of the mean and reaction rate. Other statistics do tend to lie between the limits but this is not always so, as in the case of the reactant r.m.s. and covariance values. The reactants show a trend to greater reactedness with axial distance. A lower bound on the reactant means is obtained from the reaction-dominated limit which is found by assuming instantaneous mixing to the downstream mixture fraction at the commencement of the plume, followed by reaction for the time of convection.

When the data are compared with reactants in the reacting scalar mixing layer of Bilger *et al.* (1991), the plume reactant behaves as a reactant not in excess, whereas the ambient reactant generally behaves as a reactant in excess. This behaviour is not as pronounced on the centreline where dips in the ambient reactant r.m.s. profiles with low scalar intermittency (i.e. no unmixed fluid present) indicate that the mixing process only brings a relatively small amount of ambient reactant into the centre of the plume. The results generally indicate that in the region of these measurements, which is relatively close to the grid, the plume reactant (NO) is not in excess and consequently tends to be close to its equilibrium value. These findings indicate that in modelling plumes the plume reactant may be calculated from its equilibrium value whereas this may not be the case for the ambient reactant.

The reactant covariance is found to lie beyond its equilibrium limit. This is most pronounced on the centreline and upstream. The reactant correlation coefficient is found to be approximately −0.80 across the centre of the plume which is consistent with values found in other reacting flows including atmospheric measurements. The intensity of segregation is found to have a negative value similar to that reported by Bilger *et al.* (1991), which is as expected in non-premixed flows and unlike that of Komori & Ueda (1994) who found positive values in imperfect non-premixed

conditions. The coherence of reactants at frequencies where the maximum dissipation is occurring is still high and it remains so up to the cut-off frequency of the instruments. The reaction rate is overestimated by about 15% using the Toor (1969) closure downstream but the error is up to 65% closer to the grid, because conditions are further from equilibrium there.

Turbulent scalar diffusivity is calculated by Taylor's diffusion theory and was close to that found in other similar flows. The scalar dissipation is estimated from the variance flux and the ratio of the timescales of kinetic energy dissipation and scalar dissipation, a_χ, was found to be close to that found in other similar flows.

REFERENCES

ANAND, M. S. & POPE, S. B. 1985 Diffusion behind a line source in grid turbulence. *Turbulent Shear Flows 4* (ed. L. J. S. Bradbury, F. Durst, B. E. Launder, F. W. Schmidt & J. H. Whitelaw), pp. 46–61. Springer.

BANGE, P. 1993 Hidden photostationary equilibrium: a case study on the effect of monitor averaging on the calculated oxidation rate of NO to NO_2 in the plume of a power plant. *Atmos. Environ.* 27A, 573–580.

BENDAT, J. S., & PIERSOL, A. G. 1971 *Random Data: Analysis and Measurement Procedures.* Wiley Interscience.

BILGER, R. W. 1976 Turbulent jet diffusion flames. *Prog. Energy Combust. Sci.* 13, 101-135.

BILGER, R. W. 1980a Turbulent flows with non-premixed reactants. In *Turbulent Reacting Flows* (ed. P. A. Libby & F. A. Williams), pp. 65–113. Springer.

BILGER, R. W. 1980b Perturbation analysis of turbulent nonpremixed combustion. *Combust. Sci. Technol.* 22, 251–61.

BILGER, R. W. 1993 Conditional moment methods for turbulent reacting flow. *Phys. Fluids* A 5, 436–444.

BILGER, R. W., MUDFORD, N. R. & ATKINSON, J. D. 1985 Comments on 'Turbulent effects on the chemical reaction for a jet in a nonturbulent stream and for a plume in a grid-generated turbulence' [*Phys. Fluids* 27, 77–86]. *Phys. Fluids* 28, 3175–3177.

BILGER, R. W., SAETRAN, L. R. & KRISHNAMOORTHY, L. V. 1991 Reaction in a scalar mixing layer. *J. Fluid Mech.* 233, 211–242.

BREIDENTHAL, R. E. 1979 Structure in turbulent mixing layers and wakes using a chemical reaction. *J. Fluid Mech.* 109, 1-24.

BREMHORST, K., KREBS, L., MÜLLER, U. & LISTIJONO, J. B. H. 1989 Application of a gradient diffusion and dissipation timescale ratio model for prediction of mean and fluctuating temperature fields in liquid sodium downstream of a multi-bore jet block. *Intl J. Heat Mass Transfer* 32, 2037–2046.

BRITTER, R. E., HUNT, J. C. R., MARSH, G. L. & SNYDER, W. H. 1983 The effects of stable stratification on turbulent diffusion and the decay of grid turbulence. *J. Fluid Mech.* 127, 27–44.

BROADWELL, J. E. & BREIDENTHAL, R. E. 1982 A simple model of mixing and chemical reaction in a turbulent shear layer. *J. Fluid Mech.* 125, 397–410.

BROADWELL, J. E. & MUNGAL, M. G. 1991 Large-scale structures and molecular mixing. *Phys. Fluids* A 3, 1193–1206.

BUILTJES, P. J. H. 1983 A comparison between chemically reacting plume models and wind tunnel experiments. In *Air Pollution Modelling and its Application 11* (ed. C. de Wispelaere), pp. 59–84. Plenum Press.

CHENG, L., PEAKE, E., ROGERS, D. & DAVIS, A. 1986 Oxidation of nitric oxide controlled by turbulent mixing in plumes from oil sands extraction plants. *Atmos. Environ.* 20, 1697–1703.

CORRSIN, S. 1961 The reactant concentration spectrum in turbulent mixing with a first order reaction. *J. Fluid Mech.* **11**, 407–416.

CORRSIN, S. 1964 Further consideration of Onsager's cascade model for turbulent spectra. *Phys. Fluids* **7**, 1156–1159.

DELANY, A. C., FITZJARRALD, D. R., LENSCHOW, D. H., PEARSON, R., WENDEL, G. J. & WOODRUFF, B. 1986 Direct measurements of nitrogen oxides and ozone fluxes over grassland. *J. Atmos. Chem.* **4**, 429–444.

FACKRELL J. E. & ROBINS, A. G. 1982 Concentration fluctuations and fluxes in plumes from point sources in a turbulent boundary layer. *J. Fluid Mech.* **117**, 1–26.

GAD-EL HAK, M. & MORTON, J. B. 1979 Experiments on the diffusion of smoke in isotropic turbulent flow. *AIAA J.* **17**, 558–562.

GERHKE, P. J. & BREMHORST, K. 1993 Lateral velocity fluctuations and dissipation timescale ratios for prediction of mean and fluctuating temperature fields. *Intl J. Heat Mass Transfer* **36**, 1943–1952.

GIBSON, M. M., JONES, W. P. & KANELLOPOULOS, V. E. 1989 Turbulent temperature mixing layer; measurement and modelling. In *Turbulent Shear Flows 6* (ed. J.-C. Andre, J. Cousteix, F. Durst, B. Launder, F. Schmidt & J. Whitelaw), pp. 119–128. Springer.

HINZE, J. O. 1975 *Turbulence*, 2nd edn. McGraw-Hill.

IBRAHIM, S. S. 1987 Nonequilibrium chemistry in a turbulent smog chamber. PhD thesis, University of Sydney.

JAYESH & WARHAFT, Z. 1992 Probability distribution, conditional dissipation, and transport of passive temperature fluctuations in grid generated turbulence. *Phys. Fluids* A **4**, 2292–2307.

KAMP DE FERIET, J. 1938 Some recent researches on turbulence. In *Proc. 5th Intl Congr. Appl. Mech. Cambridge, MA*, pp. 558–355.

KERSTEIN, A. L. 1992 Linear-eddy modelling of turbulent transport. Part 7. Finite-rate chemistry and multi-stream mixing. *J. Fluid Mech.* **240**, 289–313.

KLIMENKO, A. YU. 1990 Multicomponent diffusion of various admixtures in a turbulent flow. *Fluid Dyn.* **25**, 327-334.

KOMORI, S., HUNT, J. C. R., KANZAKI, T. & MURAKAMI, Y. 1991 The effects of turbulent mixing on the correlation between two species and on concentration fluctuations in non-premixed reacting flows. *J. Fluid Mech.* **228**, 629–659.

KOMORI, S., NAGATA, K., KANZAKI, T. & MURAKAMI, Y. 1993 Measurements of mass flux in a turbulent liquid flow with a chemical reaction. *AIChE J.* **39**, 1611–1620.

KOMORI, S., & UEDA, H. 1984 Turbulent effects on the chemical reaction for a jet in a nonturbulent stream and for a plume in a grid-generated turbulence. *Phys. Fluids* A **27**, 77–86.

KOOCHESFAHANI, M. M. & DIMOTAKIS, P. E. 1986 Mixing and chemical reaction in a turbulent liquid mixing layer. *J. Fluid Mech.* **170**, 83–112.

KOSÁLY, G. 1993 Frequency spectra of reactant fluctuations in turbulent flows. *J. Fluid Mech.* **246**, 489–502.

LARUE, J. C., LIBBY, P. A. & SESHADRI, D. V. R. 1981 Further results on the thermal mixing layer downstream of a turbulence grid. *Phys. Fluids* **24**, 1927–1933.

LI, J. D. & BILGER, R. W. 1996 The diffusion of conserved and reactive scalars behind line sources in homogeneous turbulence. Submitted to *J. Fluid Mech.*

LI, J. D., BROWN, R. J. & BILGER, R. W. 1992 Experimental study of scalar mixing layer using reactive and passive scalars. In *Proc. Eleventh Australasian Fluid Mech. Conf., University of Tasmania*, pp. 159–162.

LI, J. D., BROWN, R. J. & BILGER, R. W. 1995 Spectral measurements of reactive and passive scalars in a turbulent reactive-scalar-mixing layer. *Turbulent Shear Flows 9*. Springer (in press).

LIBBY, P. A. & WILLIAMS, F. A. (ed.) 1980 *Turbulent Reacting Flows*. Springer.

MA, B. K. & WARHAFT, Z. 1986 Some aspects of the thermal mixing layer in grid turbulence. *Phys. Fluids* A **29**, 3114–3120.

MANSOUR, M. S., BILGER, R. W. & DIBBLE, R. W. 1990 Spatial-averaging effects in Raman/Rayleigh measurements in a turbulent flame. *Combust. Flame* **82**, 411–425.

MELL, W. E., NILSEN, V., KOSÁLY, G. & RILEY, J. J. 1993 Direct Numerical investigations of the conditional moment closure model for nonpremixed turbulent reacting flows. *Combust. Sci. Technol.* **91**, 179–186.

MELL, W. E., NILSEN, V., KOSÁLY, G. & RILEY, J. J. 1994 Investigation of closure models for nonpremixed turbulent reacting flow. *Phys. Fluids* **6**, 1331–1356.

MICKELSEN, W. R. 1960 Measurements of the effect of molecular diffusivity in turbulent diffusion. *J. Fluid Mech.* **1**, 397–400.

MYLNE, K. R., MASON, P. J. 1991 Concentration fluctuation measurements in a dispersing plume at a range of up to 1000 m. *Q. J. R. Met. Soc.* **117**, 177–206.

MUDFORD, N. R. & BILGER, R. W. 1983 A facility for the study of nonequilibrium chemistry in an isothermal turbulent flow. In *Proc. of the Eighth Australasian Fluid Mech. Conf., University of Newcastle*, pp. 7C.9–7C.12.

NAKAMURA, I., SAKAI, Y. & MIYATA, M. 1987 Diffusion of matter by a non-buoyant plume in grid-generated turbulence. *J. Fluid Mech.* **178**, 379–403.

NYE, J. O. & BRODKEY, R. S. 1967 The scalar spectrum in the viscous-convective subrange. *J. Fluid Mech.* **29**, 151–163.

PETERS, N. 1988 Laminar flamelet concepts in turbulent combustion. *Symp. (Intl) Combust. 21st*, pp. 1231–1250. Pittsburgh: Combustion Institute.

POPE, S. B. 1985 PDF methods for turbulent reactive flows. *Prog. Energy Combust. Sci.* **11**, 119–92.

POST, K. & KEWLEY, D. J. 1978 Calibration of a ozone calibration reference instrument. *Clean Air* **12**, 2–5.

PRASAD, R. R. & SREENIVASAN, K. R. 1990 Quantitative three-dimensional imaging and the structure of passive scalar fields in fully turbulent flows. *J. Fluid Mech.* **216**, 1–34.

SAWFORD, B. L. 1987 Conditional concentration statistics for surface plumes in the atmospheric boundary layer. *Boundary-Layer Met.* **38**, 209–223.

SAWFORD, B. L., FROST, C. C. & ALLAN, T. C. 1985 Atmospheric boundary-layer measurements of concentration statistics from isolated and multiple sources. *Boundary-Layer Met.* **31**, 249–268.

SHEA, J. R. 1977 A chemical reaction in a turbulent jet. *J. Fluid Mech.* **81**, 317–333.

STAPOUNTZIS, H., SAWFORD, B. L., HUNT, J. C. R. & BRITTER, R. E. 1986 Structure of the temperature field downwind of a line source in grid turbulence. *J. Fluid Mech.* **165**, 401–424.

TAYLOR, G. I. 1921 Diffusion by continuous movements. *Proc. Lond. Math. Soc.* **20**, 196–212.

TOOR, H. C. 1969 Turbulent mixing of two species with and without chemical reaction. *Indust. Engng Chem. Fund.* **8**, 655–659.

TSUNODA, H., SAKAI, I., NAKAMURA, I. & LIU, S. 1993 The effect of a circular cylinder on the diffusion of matter by a plume. *J. Fluid Mech.* **246**, 419–442.

VILA-GUERAU DE ARELLANO, J., DUYNKERKE, P. J., JONKER P. J. & BUILTJES, P. J. H. 1993 An observational study on the effects of time and space averaging in photochemical models. *Atmos. Environ.* **27A**, 353–62.

VILA-GUERAU DE ARELLANO, J., TALMON, A. M. & BUILTJES, P. J. H. 1990 A chemically reactive plume model for the $NO—NO_2—O_3$ system. *Atmos. Environ.* **24A**, 2237–2246.

WARHAFT, Z. 1984 The interference of thermal fields from line sources in grid turbulence. *J. Fluid Mech.* **144**, 363–387.

WARHAFT, Z. & LUMLEY, J. L. 1978 An experimental study of the decay of temperature fluctuations in grid turbulence. *J. Fluid Mech.* **88**, 695–684.